Terra Nova

Review Article

doi: 10.1111/ter.12041

Caveats on tomographic images

Gillian R. Foulger,[1] Giuliano F. Panza,[2,3] Irina M. Artemieva,[4] Ian D. Bastow,[5] Fabio Cammarano,[4] John R. Evans,[6] Warren B. Hamilton,[7] Bruce R. Julian,[1] Michele Lustrino,[8,9] Hans Thybo[4] and Tatiana B. Yanovskaya[10]

[1]*Department of Earth Sciences, Durham University, Durham UK;* [2]*Department of Mathematics and Geosciences, University of Trieste, Italy and the Abdus Salam ICTP-SAND Group, Trieste Italy;* [3]*Institute of Geophysics, China Earthquake Administration, Beijing China;* [4]*Department of Geography and Geology, University of Copenhagen, Denmark;* [5]*Department of Earth Science and Engineering, Imperial College, London SW7 2AZ, UK;* [6]*U.S. Geological Survey, Menlo Park California, 94025, USA;* [7]*Department of Geophysics, Colorado School of Mines, Golden Colorado, 80401, USA;* [8]*Dipartimento di Scienze della Terra, Università degli Studi di Roma La Sapienza, P.le A. Moro, 5, 00185, Rome Italy;* [9]*CNR – Istituto di Geologia Ambientale e Geoingegneria (IGAG) c/o, Dipartimento di Scienze della Terra, Università degli Studi di Roma La Sapienza, Rome Italy;* [10]*Department of Physics of the Earth, Sankt-Petersburg State University, Sankt-Petersburg Russia*

ABSTRACT

Geological and geodynamic models of the mantle often rely on joint interpretations of published seismic tomography images and petrological/geochemical data. This approach tends to neglect the fundamental limitations of, and uncertainties in, seismic tomography results. These limitations and uncertainties involve theory, correcting for the crust, the lack of rays throughout much of the mantle, the difficulty in obtaining the true strength of anomalies, choice of what background model to subtract to reveal anomalies, and what cross-sections to select for publication. The aim of this review is to provide a relatively non-technical summary of the most important of these problems, collected together in a single paper, and presented in a form accessible to non-seismologists. Appreciation of these issues is essential if final geodynamic models are to be robust, and required by the scientific observations.

Terra Nova, 0, 1–23, 2013

Introduction

Seismic tomography is the only tool available to map the deep structure of the Earth, and it comprises a pivotal element of geochemical and dynamic models of the mantle. However, seismic tomography is limited by issues that are not widely appreciated, in particular by non-seismologists. Counterintuitively, teleseismic tomography cannot image the three-dimensional structure of the mantle. In all tomography methods, the strengths of calculated anomalies depend on subjective choices of inversion parameters, but are still commonly translated directly into critical geological parameters such as temperature and density. Tomography does not return thermal or geological information, but seismological parameters and assumptions have to be used to translate seismic results into other physical parameters, e.g. temperature or convective motion. Resolution- and error-assessment methods cannot encapsulate the true errors, and are insensitive to critical experimental limitations that invalidate parts of most derived structures.

Petrology and geochemistry are indirect tools for probing the mantle. They can provide information on its composition, but with virtually no spatial resolution. Isotope geochemistry can add a fourth dimension (time). The results from seismic tomography and petrology/geochemistry are frequently combined to develop geological models of the structure and dynamics of the mantle. This endeavour is, however, fraught with difficulties. Few practitioners are equally expert in both disciplines, and often, the data from the more familiar discipline are interpreted jointly with published interpretations from the less familiar one. Tomography models are all too often assumed to provide essentially proof positive of things that the data physically cannot prove.

Here, we provide an accessible overview, aimed primarily at non-seismologists, of the main problems that limit seismic tomography. This article is not intended to be an in-depth, technical review for theoretical seismologists. That material can be found elsewhere (e.g. Dahlen and Tromp, 1998; Aki and Richards, 2002; Nolet, 2008). It is essential to appreciate the main problems inherent in many tomographic results published over the last four decades, but not obvious *prima facie*, if cross-disciplinary interpretations are to be made that are both robust and required the data.

Correspondence: Professor Gillian R Foulger, Department of Earth Sciences, University of Durham, Science Laboratories, South Road, Durham DH1 3LE, UK. Tel.: 0191 334 2314; fax: 0191 334 2301; e-mail: g.r.foulger@durham.ac.uk

Methodological problems

Tomographic methods

Tomographic methods used to image large-scale structures in the mantle may be grouped into teleseismic-, surface-wave- and whole-mantle tomography. The first two are most sensitive to shallow mantle structure. The latter is the only method that can provide spatial information about the lower mantle.

Teleseismic tomography uses the relative arrival times of seismic waves from distant earthquakes. It has resolution on the scale typically of tens of kilometres. The earliest technique of this kind is known as "ACH" (Aki-Christoffersson-Husebye, Aki *et al.*, 1977; Christoffersson and Husebye, 2011). An array of seismic stations records typically a few hundred distant earthquakes (teleseisms) from various directions and distances. Differences, relative to reference models, in the arrival times of the seismic waves across the array, are then used to determine the three-dimensional distribution of relative wave speeds beneath the array. The imaged volume typically extends down to a depth roughly equal to the breadth of the surface array, which is commonly a few hundred kilometres.

The method has been applied to a variety of geological/tectonic settings, e.g. volcanic regions, including Yellowstone, Iceland and Hawaii (Evans and Achauer, 1993; Foulger *et al.*, 2001; Wolfe *et al.*, 2009), continental rift zones (Green *et al.*, 1991; Achauer *et al.*, 1992; Bastow *et al.*, 2005, 2008), mountain ranges (Lippitsch *et al.*, 2003; Alinaghi *et al.*, 2007; Paul *et al.*, 2010; Medhus *et al.*, 2012) and cratons (Gregersen *et al.*, 2002; James *et al.*, 2003; Obrebski *et al.*, 2011; Rawlinson and Fishwick, 2012). The original experimental design, developed when computer resources were limited, was subsequently improved (e.g. Paige and Saunders, 1982; Menke, 1984; Nolet, 1985; Dahlen *et al.*, 2000). The basic method has remained fundamentally the same, however, and as a result, its shortcomings persist.

Surface-wave tomography (Cara, 1979; Woodhouse and Dziewonski, 1984) utilizes waves whose energy is concentrated near the surface. Dispersion, caused by the dependence of surface wave speed on the depth range sampled by different wavelengths, provides information over a relatively broad depth range. Many regional (e.g. Van Der Lee and Nolet, 1997; Simons *et al.*, 1999; Bruneton *et al.*, 2004; Darbyshire, 2005; Lebedev *et al.*, 2009) and global (e.g. Dziewonski, 1971a,b; Trampert and Woodhouse, 1995; Ekström *et al.*, 1997; Billien *et al.*, 2000; Shapiro and Ritzwoller, 2002; Panza *et al.*, 2007) surface-wave tomography models are now available. An important target is upper-mantle radial anisotropy, which results from the different speeds of horizontally (SH) and vertically polarized (SV) shear waves and horizontally and vertically propagating P waves (Anderson, 1965; Tanimoto and Anderson, 1984; Lévêque *et al.*, 1998; Gung *et al.*, 2003; Marone *et al.*, 2007; Kustowski *et al.*, 2008).

Whole-mantle tomography deals with the entire mantle, and as a result, the earthquakes used are inside the study volume instead of outside it. Because of this, it is free of some, but not all, of the difficulties inherent in teleseismic- and surface-wave tomography.

Structure outside the study volume cannot be ignored

In teleseismic and surface-wave tomography, attributing arrival-time anomalies entirely to local structure is equivalent to assuming that the structure outside the study volume is strictly one-dimensional (laterally homogeneous) and corresponds exactly to a "standard" Earth model. In reality, mantle heterogeneity is pervasive so that structure outside the study volume significantly affects the data (the observed arrival times). The contaminating effect of outside structure is mathematically of the same order as the effect of structure within the study volume (Masson and Trampert, 1997; B. R. Julian, G. R. Foulger, unpublished data).

In teleseismic tomography, the biasing effects of external structure can be reduced by treating the shapes and orientations of incident wave fronts as unknowns and solving for them during tomographic inversion (B. R. Julian, G. R. Foulger, unpublished data). If a plane-wave approximation is used, the forward problem turns out to be particularly simple: the change in arrival time at a seismometer is the same as the change at the original entry point of a ray into the study volume. It is not necessary to determine the change in the ray path. Whole-mantle and local-earthquake tomography methods use an equivalent approach, solving simultaneously for the locations and origin times of earthquakes and for structure (Thurber, 1993). Each earthquake adds four unknowns to the problem (three spatial co-ordinates, plus the event origin time), but the resulting matrices are sparse and special numerical methods can reduce the computational burden (Spencer and Gubbins, 1980). Using plane wavefronts in the distant-source problem is even simpler, because each event adds only three unknowns to the problem. Application of this potential improvement to existing data sets has not yet been done. In surface-wave tomography, analogous corrections are possible (Yanovskaya, 2009).

The three-dimensional structure of the target volume is not retrieved

Contrary to popular assumption, and surprisingly, teleseismic tomography does not retrieve the three-dimensional structure of the study volume. The estimates of wave-speed variations are, for each layer, *relative to that layer's average*. The absolute values of those averages remain unknown (Aki *et al.*, 1977). Two problems result from this (Léveque and Masson, 1999):

1. Wave-speed variations are known only in the horizontal directions. Variations in the vertical direction are not calculable (Section "Resolution and checkerboard tests: Perils and pitfalls" and Supporting Information).
2. Negative anomalies are often interpreted as absolute low wave speeds, whereas they may, in truth, be absolute high wave speeds if the average value of the layer is anomalously high. Similarly, positive anomalies cannot be assumed to represent absolute high wave speeds.

Difficulties in resolving the depth extent of anomalies are exacerbated by the smearing problem, that causes anomalies to be elongated along ray bundles (see Supporting Information). In the case of teleseismic tomography, ray bundles are primarily steeply dipping, and the result is artificially vertically elongated anomalies (Fig. 1). The addition of waves from local sources may improve the vertical resolution, and teleseisms and local earthquakes should be integrated, wherever feasible (Evans and Zucca, 1993; B. R. Julian, G. R. Foulger, unpublished data).

Surface-wave tomography suffers from a different set of problems.

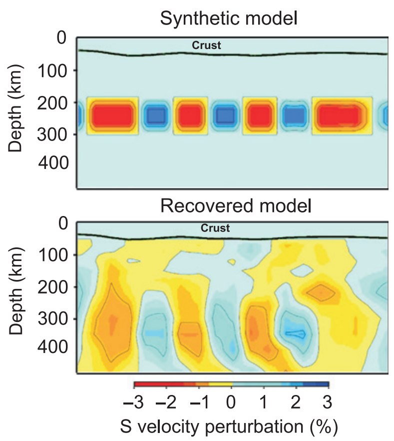

Fig. 1 Depth leakage (downward smearing) in a seismic tomography inversion (after Eken *et al.*, 2008).

Depth resolution depends critically on the data used. In the uppermost mantle, wave-speed variations within a depth range of 30–50 km are unresolvable, when only long-period waves are used and nominal depths given for both horizontal and vertical cross-sections refer to broad, often > 50-km-thick depth intervals over which wave-speed structure is integrated (Fig. 2) (Ritsema *et al.*, 2004). For teleseismic- and whole-mantle tomography, depth averaging often involves even thicker intervals. The resolution of surface-wave tomography is worst for the depth range ~300–400 km which is, inconveniently, the depth to which the deepest roots of cratonic lithosphere extend (Polet and Anderson, 1995). One consequence of this is that long-wavelength global models for the transition zone vary greatly (Cammarano *et al.*, 2011) (Fig. 3).

Correcting for the crust

All seismic stations are deployed at the surface. Thus, to extract the structure of the mantle, correction must be applied for the crust and for any part of the shallow mantle that is unresolvable because of a lack of crossing rays. In the case of teleseismic tomography, one approach is to solve for a correction for each seismic station ("station corrections" or "station terms"). Alternatively, a crustal model can be used. An example is CRUST 2.0 (Bassin *et al.*, 2000), which specifies crustal structure on a 2° × 2° grid (~225 × 225 km). The resolution of crustal models is variable, but is usually worse than 500 km except for small, local areas.

These corrections may thus be only approximately correct, but nevertheless amount to as much as half of the entire travel-time delay. They may also exceed the delays associated with structures imaged at depth and interpreted as bodies of primary significance. For example, in the teleseismic tomography study of Hawaii by Wolfe *et al.* (2009), the range of station corrections across the network was ~±3 s, whereas the residual *S*-wave arrival-time anomalies, after correction had been made, and which were used to image deeper structure, only amounted to ~2–3 s. Clearly, it is important that the appropriate corrections are accurately known, but this may be challenging.

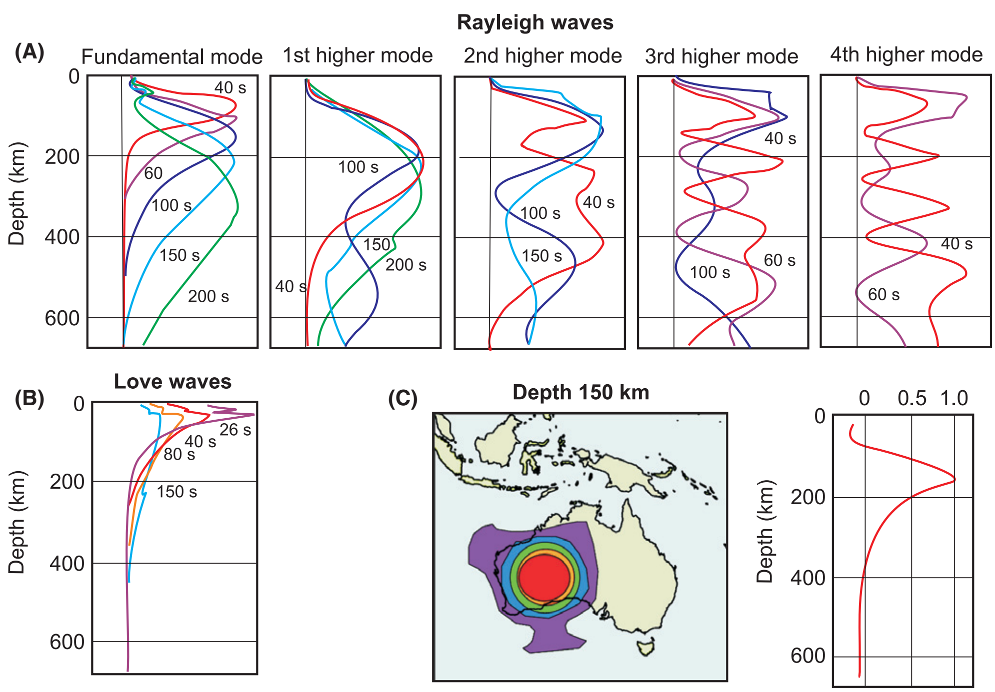

Fig. 2 (A) Sensitivity kernels (normalized to a maximum amplitude of 1) that relate Rayleigh-wave phase wave speed of the fundamental mode and the overtones to shear wave speed for the PREM model (after Ritsema *et al.*, 2004). (B) Love wave sensitivity at different periods with respect to horizontal shear wave-speed variations (after Curtis *et al.*, 1998). (C) Backus–Gilbert resolution kernels for global surface-wave tomography model S20RTS for a point beneath Australia at 150 km depth (left, lateral resolution) and the radial dependence of the resolution kernel (right, vertical averaging in the final model. After Ritsema *et al.*, 2004).

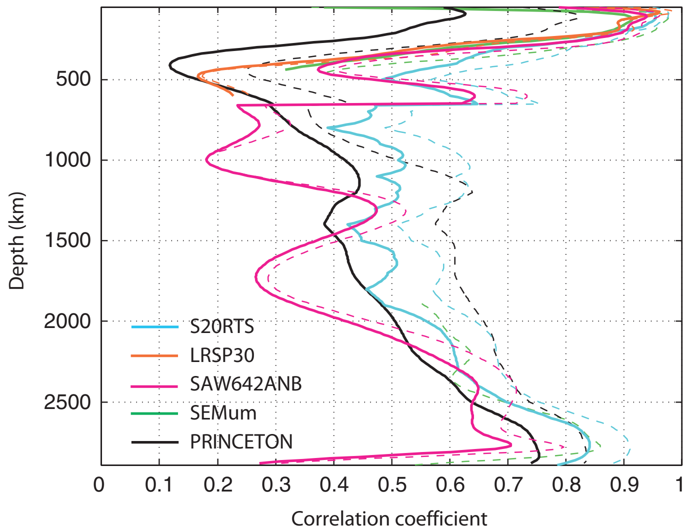

Fig. 3 Correlation coefficients between several v_S models (Cammarano *et al.*, 2011).

The problem of correcting for the crust also affects surface-wave- and whole-mantle tomography. If inadequately done, corrections based on estimated crustal structure can erroneously propagate into images of mantle structure. For example, the PREM whole-mantle model (Dziewonski and Anderson, 1981), often used as a starting model, includes a 21.4-km-thick globally averaged crust. This differs significantly from both the true oceanic and continental crust. As a result, structural artefacts can appear at tectonic boundaries (Boschi and Ekstrom, 2002; Ritsema *et al.*, 2004; Panning *et al.*, 2010).

For the longest-wavelength (>200 s) Rayleigh waves, the crustal effect is relatively small (Fig. 4) (Mooney *et al.*, 1998; Ritsema *et al.*, 2004). For waves with shorter periods, the problem is greater. For periods of 150 s, the crustal contribution may reach 50% of the total wave-speed variations, and for 40 s Rayleigh waves, the contribution may be 100% (Ritsema *et al.*, 2004; Artemieva, 2011). Heterogeneities such as large sedimentary basins or calderas may have a significant effect. For Rayleigh waves with periods of 35 s, an error in estimated basin thickness of only 1 km may produce a 1% error in mantle phase wave speeds (Bassin *et al.*, 2000). Low-density ice sheets can also have strong effects (Fig. 4) (Ritzwoller *et al.*, 2001).

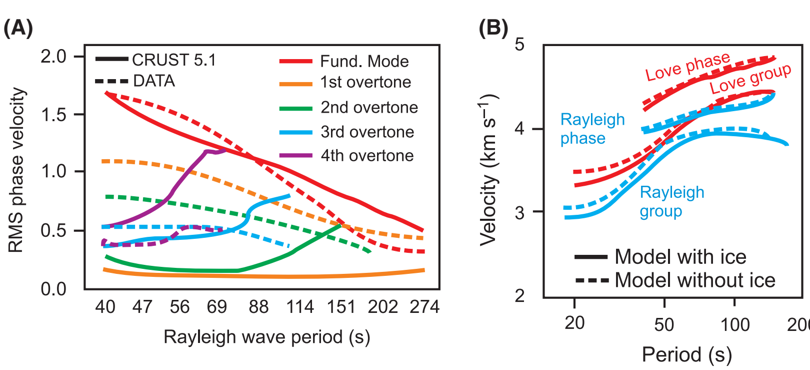

Fig. 4 (A) Root-mean-square phase wave-speed perturbation of the Rayleigh wave with respect to PREM (in %) in the data (dashed lines) and produced by crustal correction (solid lines) for the CRUST 5.1 model (Mooney *et al.*, 1998; Ritsema *et al.*, 2004), (B) the effect of the ice sheet on surface wave velocities (after Ritzwoller *et al.*, 2001).

Anomaly amplitudes cannot be reliably determined

Anomaly amplitudes calculated using all tomographic methods are heavily dependent on relatively arbitrary aspects of the inversion process (Song and Helmberger, 2007). Figure 5 shows, for example, different teleseismic tomography models for mantle structure at 165 km beneath Ireland (O'Donnell *et al.*, 2011). The rightmost upper two models achieve essentially the same goodness of fit to the data (i.e. RMS data misfit reduction, shown on the vertical axis of the graph lowermost). Nevertheless, the amplitudes of the anomalies obtained are radically different.

The amplitudes calculated can be varied at will or unknowingly, by changing inversion program input parameters in ways that do not materially affect the data fit. Factors may include weightings of the different datasets included in the inversion, choice of damping factors and model smoothness, and the mathematical way in which the study volume is described, e.g. whether uniform blocks or wave-speed gradients between grid points are used. In addition, the depth to the base of the study volume must be chosen, whether or not to use station corrections and how to correct for the crust. Synthetic tests can rarely reproduce the amplitudes of velocity perturbations in input models (Fig. 1) (Eken *et al.*, 2008; Christoffersson and Husebye, 2011).

The tomographic inversion problem is inherently and always underdetermined, i.e. there are fewer data than model unknowns. Thus, it is impossible to find a unique solution. This problem is typically addressed using "regularization" (Trampert and Spetzler, 2006). A final model is chosen that most closely matches the initial model estimate (e.g. Aki *et al.*, 1977; Tarantola, 1987), for example, by damping the amplitudes of anomalies with respect to the starting one-dimensional velocity model (e.g. Evans and Achauer, 1993).

A trade-off curve provides a selection of models to choose from, but deciding precisely which model is best is somewhat *ad hoc*. Sometimes the knee of the trade-off curve is preferred, and sometimes *a priori* estimates of data error govern the final

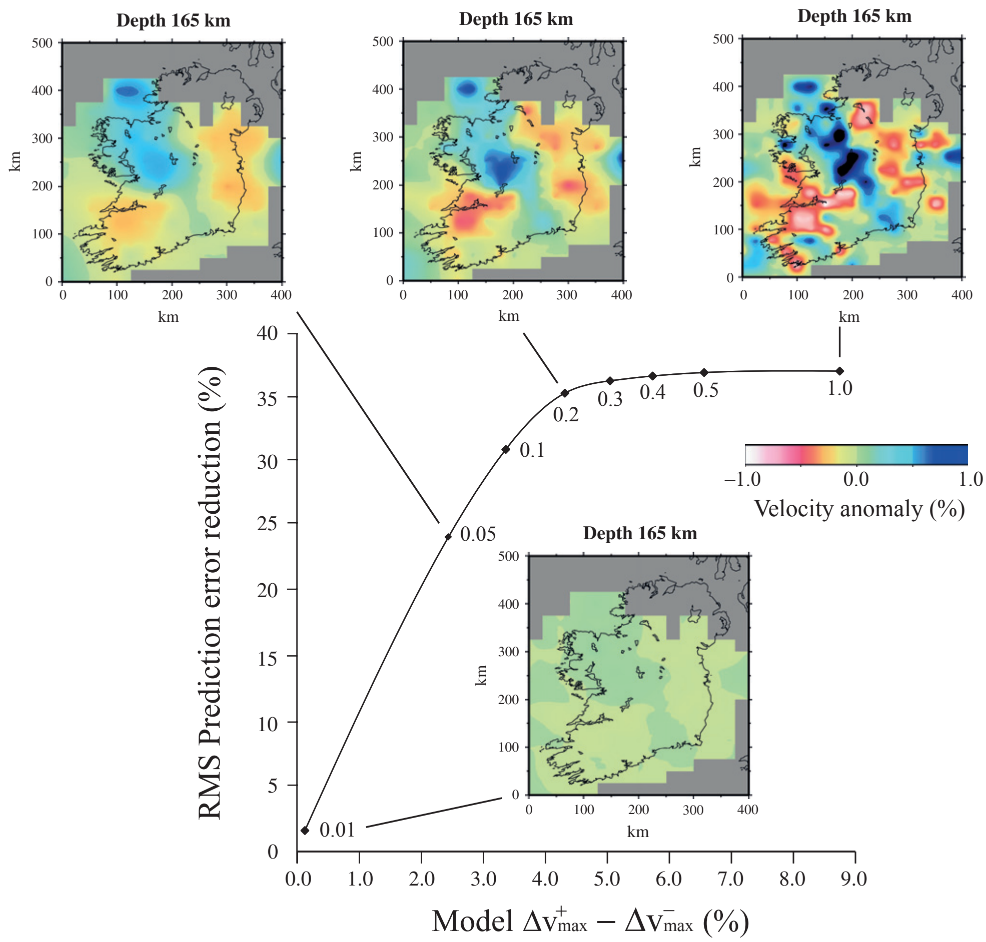

Fig. 5 Trade-off curve showing the balance between model roughness (quantified by the difference between the extremal positive and negative wave-speed contrasts, $\Delta v^{+}_{max} - \Delta v^{-}_{max}$) and root mean square prediction error reduction (%). The curve is labelled with wave-speed model parameter standard deviations. Each point represents a model solution corresponding to the indicated model parameter standard deviations (from O'Donnell *et al.*, 2011).

choice (Fig. 4 from the study of O'Donnell *et al.*, 2011). In most published tomographic studies, model dependence on regularization is not displayed, so the information required to judge the reliability of the chosen image is not available.

It is popular to apply the principle of Occam's razor to select smoothly varying models (e.g. Boyadzhiev *et al.*, 2008). This, however, only guarantees that the wave-speed amplitudes will be underestimated. Smoothing is achieved using the average of adjacent blocks, and this suppresses the amplitudes of small, high-gradient features (Fig. 6). A further disadvantage of this is that blocks containing no rays are interpolated or extrapolated to the grid edges, producing wave-speed perturbations in regions that may contain no data. Smoothing can also be done at the plotting stage by interpolating the wave speeds between homogenous blocks and using a continuous colour spectrum.

True amplitudes can be distorted in surface-wave tomography by limited lateral resolution (Fig. 2C) (Ritsema *et al.*, 2004). At 150 km depth beneath Australia, for example, lateral resolution of the S20RTS surface-wave model (Ritsema *et al.*, 1999) is almost half the continent in width, and includes oceanic, Archean and Proterozoic provinces. The problems are revealed when independent groups perform inversions using similar datasets, and obtain very different anomaly amplitudes. An example is inversions for the structure of the Western USA mantle, using USArray data (Sun and Helmberger, 2011; Becker, 2012).

Efforts have been made in recent years to improve anomaly amplitude recovery using various approaches. However, the inherently underdetermined nature of tomographic inversions means that some form of damping or smoothing is invariably required. Thus, amplitude recovery is likely to always remain problematic.

Inhomogeneous ray coverage

The Earth's mantle is not uniformly sampled by seismic waves. Earthquakes are concentrated in narrow belts, and most are shallow, *i.e.*, in the upper few hundred kilometres. Only in a few regions do they occur as deep as the transition zone, and very few occur beneath the 670-km discontinuity (Anderson, 1967, 2007; Hamilton, 2007). All seismic stations

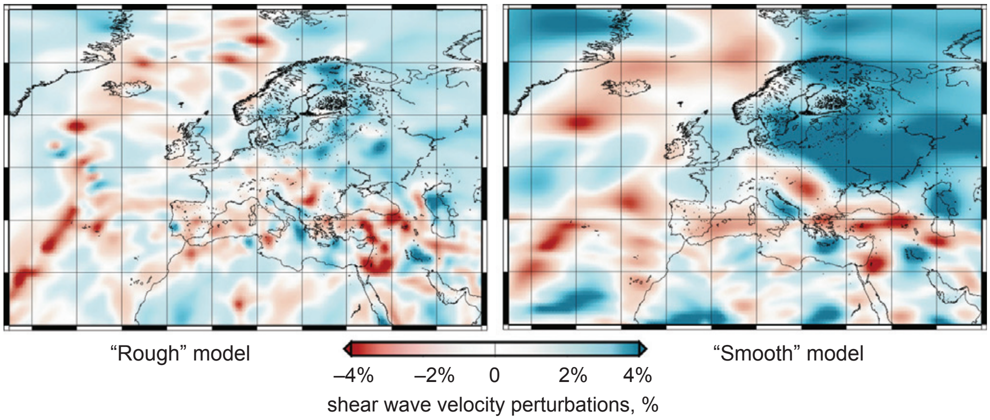

Fig. 6 The effect of smoothing on mantle velocity structure. The example refers to 110 km depth. The model is constrained by non-linear waveform inversion (Legendre *et al*., 2012).

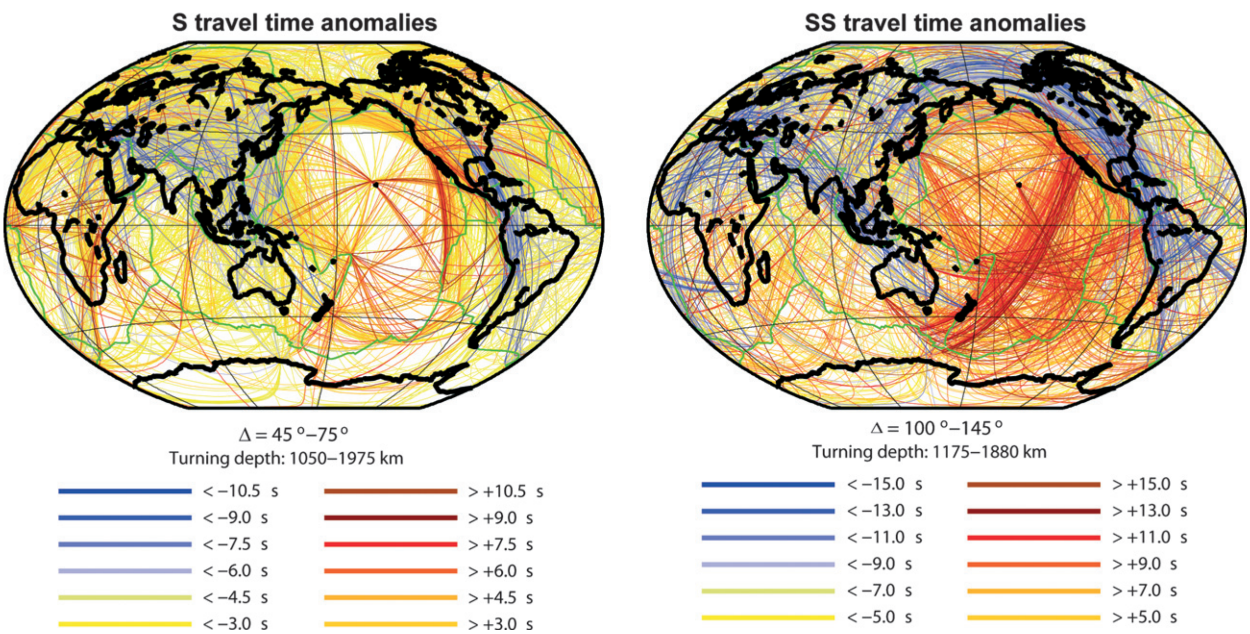

Fig. 7 *S* and *SS* raypaths sampling the mid-mantle. Much of Earth's interior is effectively unsampled and much else is sampled primarily by sub-parallel rays rather than by the diversely crossing rays required for good tomographic imaging. The so-called deeply subducted "Farallon slab" (Grand *et al*., 1997) beneath the Caribbean and eastern United States is particularly non-uniformly sampled. Published tomographic images of this region vary greatly (Fig. 11). (Figure provided by Jeroen Ritsema and published in Hamilton, 2011).

are deployed at the Earth's surface, mostly on land, with few on the sea floor. As a result, the distribution of measurable seismic rays (i.e., seismic waves travelling from earthquakes to stations) in the mantle is non-uniform, and so also is the ability of tomography to reveal structure (Fig. 7).

This problem leads to two major difficulties:

1 The structure of much of the mantle is essentially unobtainable. In inversions, wave speeds in these regions are not significantly perturbed from the hypothetical starting model. Unfortunately, most colour illustrations of tomographic images do not distinguish between regions where the wave speed is confidently determined to be the same as the starting value, and regions where the starting value is retained because of lack of data (Section "Displaying the results"). Apparent anomalies in the resulting images may thus correspond to those volumes where seismic rays exist, because only there can inversions change the initial starting value. Some apparently narrow, restricted anomalies may thus simply be those portions of wide anomalous regions that happen to contain rays.

2 Some regions may be sampled only by quasi-parallel bundles of mostly parallel rays. An example of this problem from teleseismic tomography is a study done at Hawaii, where a deep, low-wave-speed anomaly interpreted as a plume is

dependent only on steeply upcoming SKS waves (waves that pass through the core; right panel, Fig. 8). This ray bundle is approximately colinear to the body illustrated, and the data could equally well be explained by structure outside the study volume or at shallower depth, somewhere along the ray-bundle path.

The Hawaii region is difficult to study using teleseismic tomography because it is essentially equidistant from most parts of the distant, circum-Pacific, seismogenic plate boundaries. Recorded earthquakes thus tend to have similar epicentral distances and angles of approach and arrive beneath Hawaii with a skirt-like distribution. The travel-time corrections necessary for the exceptionally thick igneous crust and lithosphere are greater than some associated with underlying mantle anomalies for which significance is claimed. Thus, a relatively small percentage error in these corrections could profoundly change the result (Section "Correcting for the crust"). The mantle throughout the Pacific has exceptionally low wave speeds compared with the global average, complicating the choice of an appropriate *a priori* model (Gu *et al.*, 2001a,b).

Inhomogeneous sampling is a major problem in whole-mantle tomography. Figure 9 shows images interpreted as deep-mantle plumes beneath various ocean islands (Montelli *et al.*, 2004a,b, 2006). These "anomalies" are likely artefacts of quasi-parallel, upward-travelling ray bundles recorded on island seismic stations that are surrounded by large oceanic regions devoid of stations, and thus also devoid of recorded seismic waves. As a result, a one-to-one correspondence between observed "plume-like" anomalies and ocean-island seismic stations was produced (van der Hilst and de Hoop, 2005). In the case of surface-wave tomography, linear "artefact anomalies" appear in models along the dominant, horizontal ray directions (Fig. 10) (van der Lee *et al.*, 2001; Feng *et al.*, 2007).

Resolution and checkerboard tests: Perils and pitfalls

Teleseismic tomography is valid at most to a depth about equal to the aperture of the observational array, and then only when the ray set used is uniformly distributed in location and orientation. Both measures of ray homogeneity apply individually

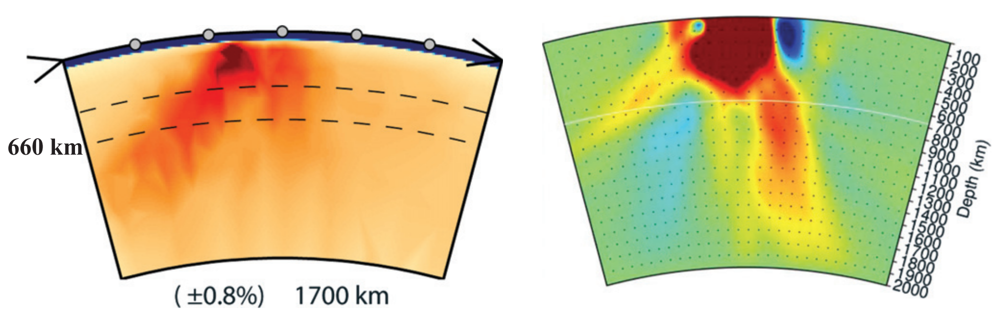

Fig. 8 An example of the absence of repeatability. Two tomography images, each showing a downward-elongated low wave-speed region beneath Hawaii. Each profile is approximately 3000 km long and each runs from NW (left end) to SE (right end) along the Hawaiian volcanic chain. One plunges to the north-west and the other to the south-east. Both were interpreted as a mantle plume (left; Li *et al.*, 2008; right, Wolfe *et al.*, 2009).

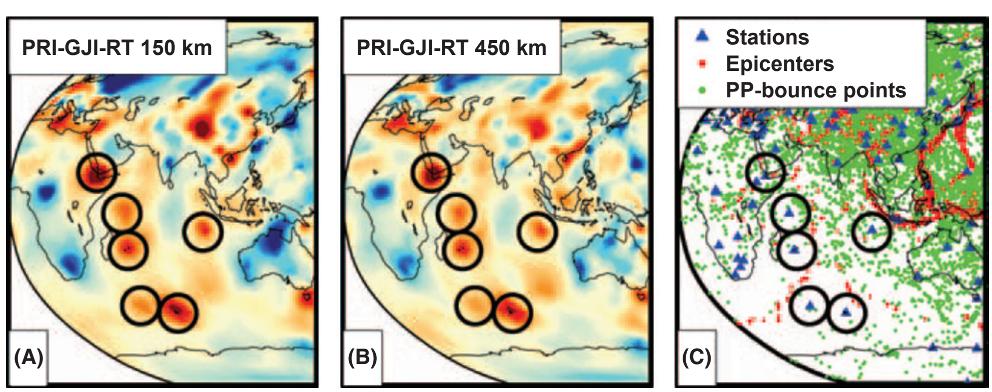

Fig. 9 Map of v_P at 150 km (left) and 450 km depth (middle) beneath the Indian Ocean according to model PRI-GJI-FFT (Montelli *et al.*, 2004a,b, 2006). They are almost identical, suggesting that they arise from quasi-parallel bundles of up-coming rays. The geographical distribution of sources (red dots), receivers (blue triangles) and *PP* bounce points (green dots) depicted in the right panel shows that ray sampling is sparse in much of the Indian Ocean except immediately beneath seismic stations deployed on islands (from van der Hilst and de Hoop, 2005; see also http://www.mantleplumes.org/BananaDoughnuts.html).

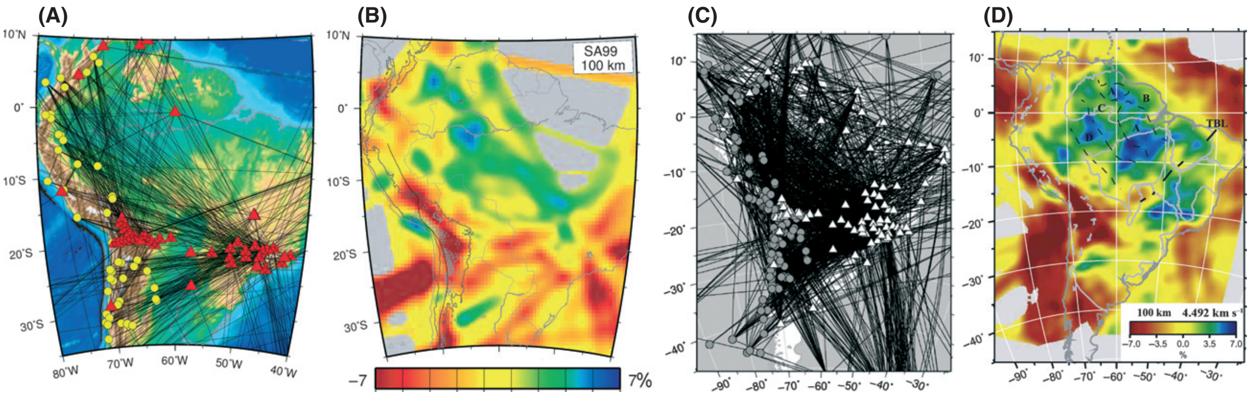

Fig. 10 Wave-speed perturbations with respect to IASP91 (Kennett and Engdahl, 1991) at 100 km depth beneath South America (B, D) and the corresponding raypaths for Rayleigh waveform data (A, C) (C-D from Feng *et al*., 2007; A-B from van der Lee *et al*., 2001).

at every location in the modelled volume and affect neighbouring volumes. Deeper and peripheral features in the inversion result are in all cases unreliable and should not be interpreted. Checkerboard tests of **R** are optimistic and misleading because they are optimal for damped inverses (van der Hilst *et al*., 1993; Léveque *et al*., 1993) (see Supporting Information).

Cryptic problems derive from the approximations, parameterization, damping, linearization and finiteness of the ray set used. In short, they derive from the numerous differences between the true Earth structure and its approximation by all types of tomography. In addition, current methods of measuring seismic travel times (VanDecar and Crosson, 1990) subsume systematic errors that then map into calculated models and are effectively impossible to quantify or to recognize in the results.

The common failure to understand and deal with these problems has led to a number of unsupportable claims of deep, narrow wave-speed anomalies interpreted as plumes extending well into the lower mantle, and even as far as the core-mantle boundary (Bijwaard and Spakman, 1999; Montelli *et al*., 2004a,b, 2006; Yuan and Dueker, 2005; Wolfe *et al*., 2011). While teleseismic tomography cannot eliminate the possibility that such anomalies exist, neither can it confirm them, nor provide relevant constraints. The only test we are aware of that can demonstrate the presence of deep, low wave-speed conduits is by using steep rays to search for guided waves – so-called "fibre optic" modes (Julian and Evans, 2010). While this test could be attempted with several existing data sets, it has not, to our knowledge, so far been done.

Lack of consideration of resolution leads to anomalies that are too small or too weak to have been resolved (*i.e.* are simply noise or artefacts) being presented in published images and interpreted. This can lead to the use of unreliable tomographic images as support for assumptions, rather than to the use of reliable features to test hypotheses. An example is the widespread use of unresolved images to bolster the concept that volcanic areas are fed by hot, rising diapirs. Alternative, shallow-based models to explain migrating- and large-volume volcanic systems have been suggested. These include water in the mantle near ridges or transform faults (Bonatti, 1990), shear heating at the base of the lithosphere (Shaw, 1973; Doglioni *et al*., 2005; Anderson, 2011), the effect of adjacent glaciers (Carminati and Doglioni, 2010) and instabilities produced by cold, down-welling material (Davies and Bunge, 2006).

A second example is the thickness of the cratonic LID. A number of studies argue it is no thicker than 200–250 km (e.g. Gung *et al*., 2003). However, such conclusions are unsafe because models based on fundamental surface-wave modes lose resolution at 200–300 km depth (Fig. 2) and vertical structure cannot be resolved better than 30–50 km.

Repeatability

If a feature imaged by tomography is reliable, it should be resolvable in multiple independent studies. Geological significance should only be attributed to features detected in all reputable studies (Foulger *et al*., 1995; Shapiro and Ritzwoller, 2002). Figure 8 illustrates this problem at Hawaii. There, two independent studies both resolved a strong, low wave-speed anomaly in the upper mantle (Li *et al*., 2008; Wolfe *et al*., 2009). This part of the two images may be considered reliable, at least in location and sign. On the other hand, the trajectory of downward-continuing low wave speeds into the lower mantle are almost exact mirror images in the two studies. These bodies and even the very existence of a downward continuation of the upper-mantle, low-wave-speed anomaly are unreliable.

Tomographic models of the purported whole-mantle-crossing "Farallon slab" are shown in Fig. 11. This structure is frequently cited as the strongest evidence available for the sinking of slabs to the core-mantle boundary (e.g. Kellogg and Wasserburg, 1990). Nevertheless, the shape of the lower mantle, high-wave-speed anomaly is very different between different results. It is a feature of global extent, too large to be explained as a single subducted slab, in particular when slab thermal- and compositional re-equilibrium with the mantle are considered. The true extent and geological nature of much of this anomaly remain uncertain.

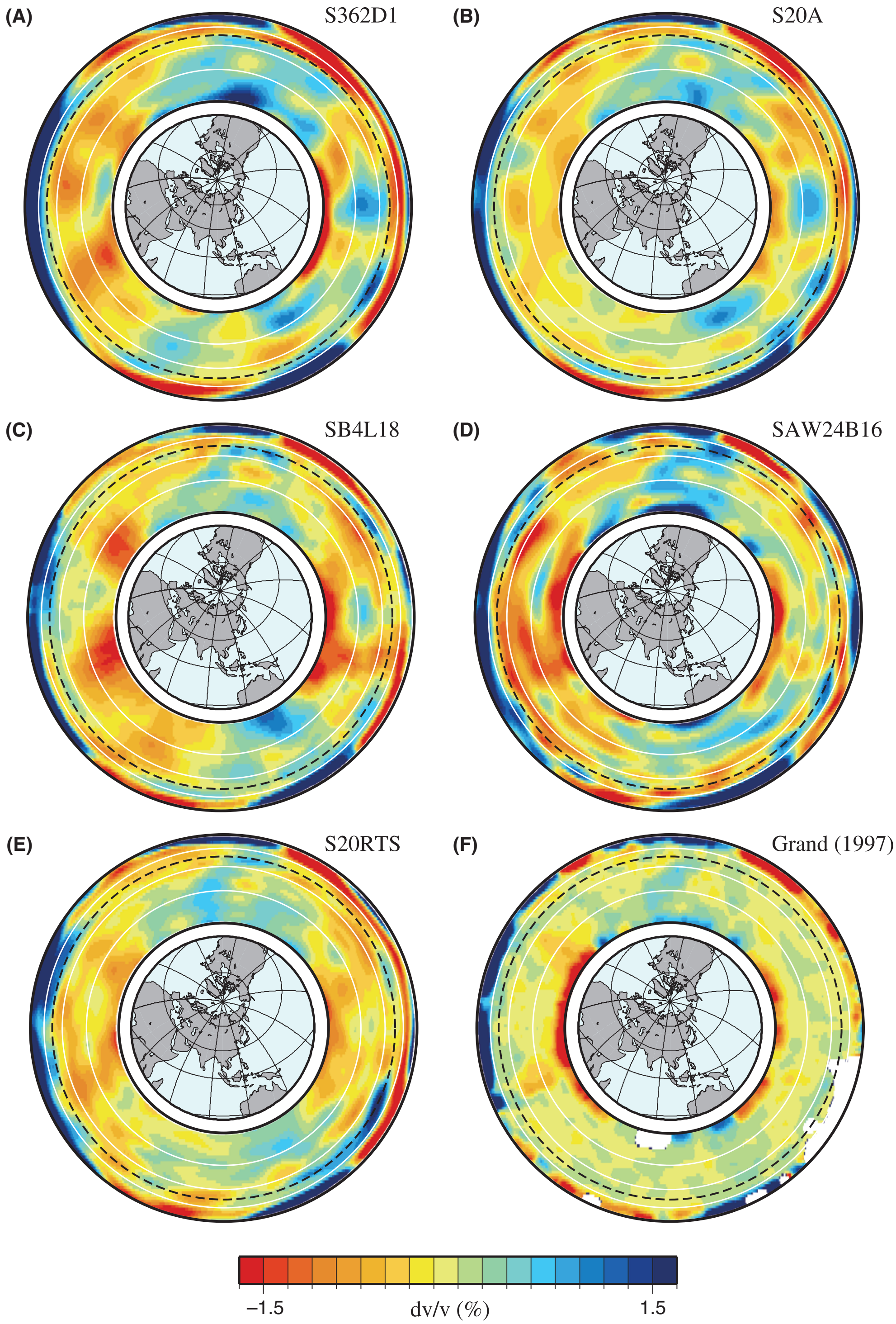

Fig. 11 Cross-sections from six whole-mantle tomography models. The complex wave-speed pattern under North America and the eastern Pacific is very variable from model to model. Support for different models of mantle structure and dynamics can be claimed, simply by choosing a preferred result (from Gu *et al.*, 2001a,b).

Only in a few cases have formal uncertainties in tomographic results been published (e.g. Panza *et al.*, 2007; Brandmayr *et al.*, 2010; Corchete and Chourak, 2010, 2011; Raykova and Panza, 2010; Gonzales *et al.*, 2011). If uncertainties were published routinely, many seismic anomalies interpreted geologically, widely used in undergraduate teaching, and relied upon to support geochemical and geodynamic models, would be recognized as noise or artefacts (Shapiro and Ritzwoller, 2002).

Absolute and relative wave speeds

Teleseismic tomography retrieves only *relative* wave speeds. The method cannot recover absolute wave speeds, and the mean anomaly of the final result is constrained to be zero relative to the reference model. These facts profoundly influence how the results are typically illustrated and, as a result, interpreted.

Illustrations commonly comprise colour maps and cross-sections showing either the relative anomalies as percent deviation from the original starting model, or absolute wave speeds determined by adding the relative anomalies back into the starting model. It is critical to understand a number of issues with these illustrative approaches if the results are to be understood correctly, even where they are well constrained.

Interpreting relative anomalies

Colour plots typically show positive (fast) and negative (slow) anomalies relative to a "zero" contour that corresponds approximately to the mean wave speed in each individual layer (Bastow, 2012). Such a plot is *constrained* to contain approximately equal volumes of positive and negative anomalies. This illustration style encourages the perception that the positive and negative anomalies are relative to some global average. Such a perception is almost always wrong. Figure 12 shows the global tomographic model of Ritsema *et al.* (2011) compared with two regional tomographic studies, one from Canada (Frederiksen *et al.*, 2007) and the other from Ethiopia (Bastow *et al.*, 2008). The "zero contours" in the two regions clearly correspond to radically different absolute wave speeds. In the case of the Canada study (left), the average wave speed relative to a global mean (middle) is high. The opposite applies to the Ethiopia study. There, relative to the global mean, wave speeds in the region are extremely low – as much as 6% low, and amongst the lowest for any continental area (Bastow *et al.*, 2005, 2008). Despite appearances, white regions are not "normal" compared with the global mean, and blue/red regions are not anomalously fast/slow. This problem can propagate into physical interpretations, by encouraging interpretation in terms of physical properties that are low or high relative to a global average, e.g. temperature.

Different interpretations of relative arrival-time tomographic images have, for example, resulted in markedly different tectonic interpretations of tomographic studies in Ireland and the British Isles. Arrowsmith *et al.* (2005) suggested that absolute delay times in the UK are late with respect to the global mean, and interpreted low-velocity anomalies as evidence for elevated mantle temperatures beneath the region. Wawerzinek *et al.* (2008) drew similar conclusions for the Irish mantle. In contrast, O'Donnell *et al.* (2011) cited evidence from global (Ritsema *et al.*, 2011) and regional surface-wave models (measures of absolute wavespeed; e.g. Pilidou *et al.*, 2004, 2005), and more recent catalogues of absolute travel-time delays (Amaru *et al.*, 2008) to suggest that the background mean wave-speed in the UK/Ireland is, in fact, fast compared with the global mean, precluding the need for a high-temperature, partial-melt hypothesis to explain wave-speed variations beneath the region.

Relative wave-speed plots impart radically different visual impressions from absolute wave-speed plots, which depict true Earth seismic structure (Section "Interpreting absolute wave speeds"). Figure 13 compares an absolute global wave-speed model (bottom) with wave-speed perturbations relative to the background model used (middle). The most significant and reliable features are not visible in the relative model, including the global, upper-mantle low-velocity zone (LVZ) (Thybo, 2006). Similar plots for southern Africa are

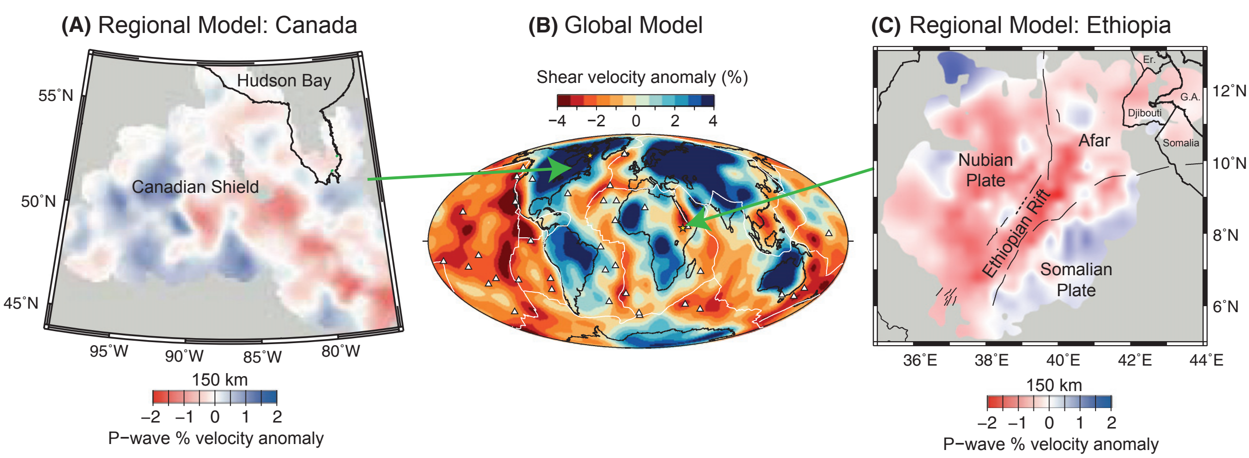

Fig. 12 Comparison of global and regional tomographic models. (A) Slice at 150-km-depth through the v_P relative arrival-time tomography model of Frederiksen *et al.* (2007) in Canada, computed from the inversion of relative arrival-time residuals. (B) Slice at 150-km-depth through the global tomographic model of Ritsema *et al.* (2011). White lines are plate boundaries. (C) Slice at 150-km-depth through the v_P relative arrival-time tomography model of Bastow *et al.* (2008) in Ethiopia, computed from the inversion of relative arrival-time residuals. Dark lines are mid-Miocene border faults that define the Ethiopian Rift. Areas of poor ray coverage are grey (from Bastow, 2012).

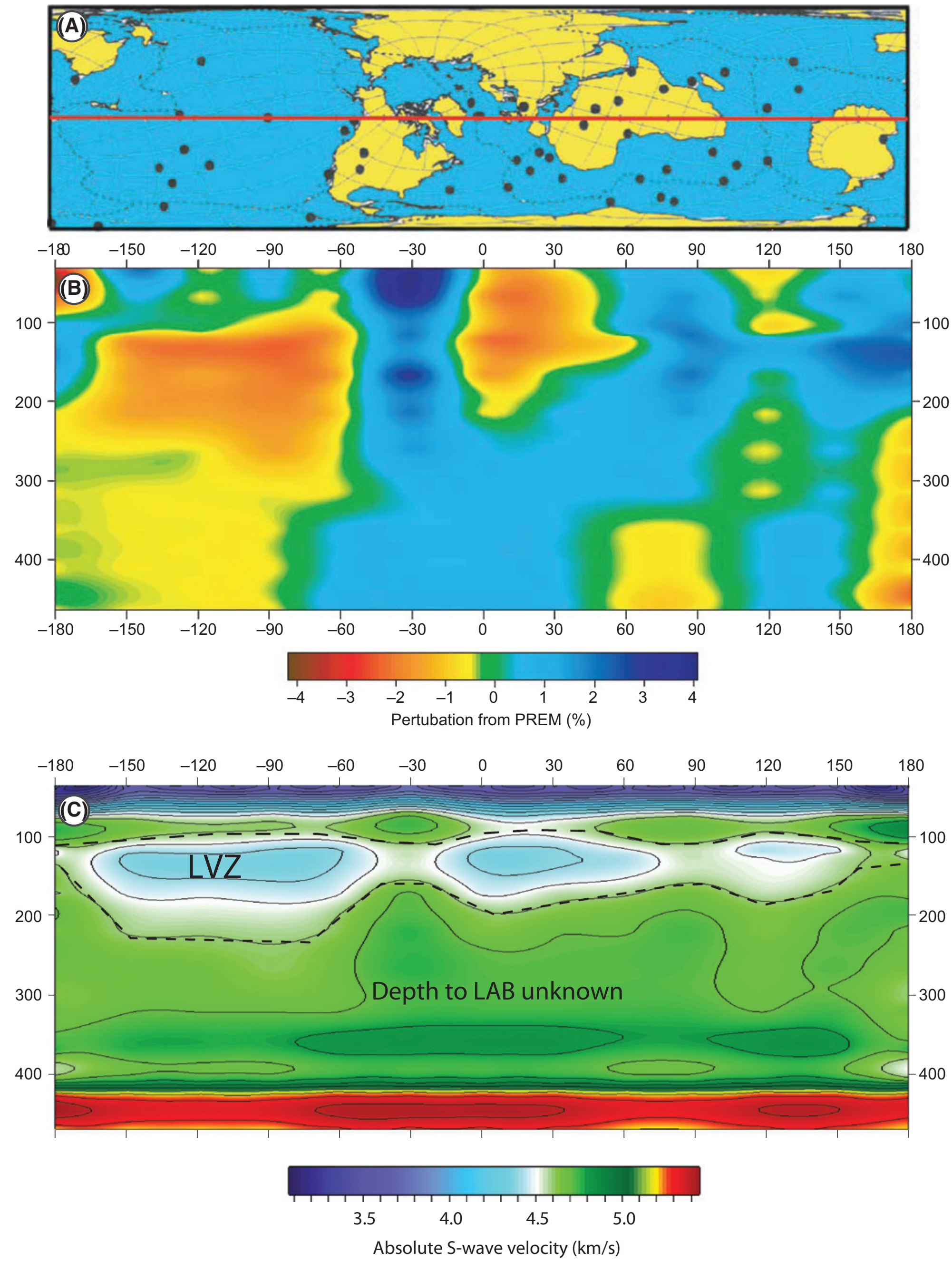

Fig. 13 Global travel-time inversion results from Zhang and Tanimoto [1993]. A) Map of the cross-section profile, B) wave-speed perturbations relative to the background model (PREM). This figure does not show any indication of an upper-mantle LVZ. Instead, it shows abrupt wave-speed discontinuities between continents and oceans. C) Absolute wave speeds calculated by adding the perturbations to the background model. This figure clearly shows a pronounced, global LVZ which is strongest beneath the oceans and extends beneath the continents. This feature is not seen in B). The amplitude of the anomaly in terms of absolute wave speed may be over-estimated due to smearing and smoothing in the inversion procedure (modified from Thybo, 2006).

shown in Fig. 14, and for Siberia in Fig. 15.

Interpreting absolute wave speeds

Absolute wave speeds are derived by adding the relative anomaly results to some "average" seismic model. Thus, the choice of model is influential. Figure 14 shows cross-sections of southern Africa in the form of (a) absolute wave speeds and (b–c) anomalies relative to two different global seismic models. Although careful inspection reveals common features between the three cross-sections, at first glance, they look radically different and there is clearly risk of misinterpretation. This risk would be higher if only one cross-section were published, and even

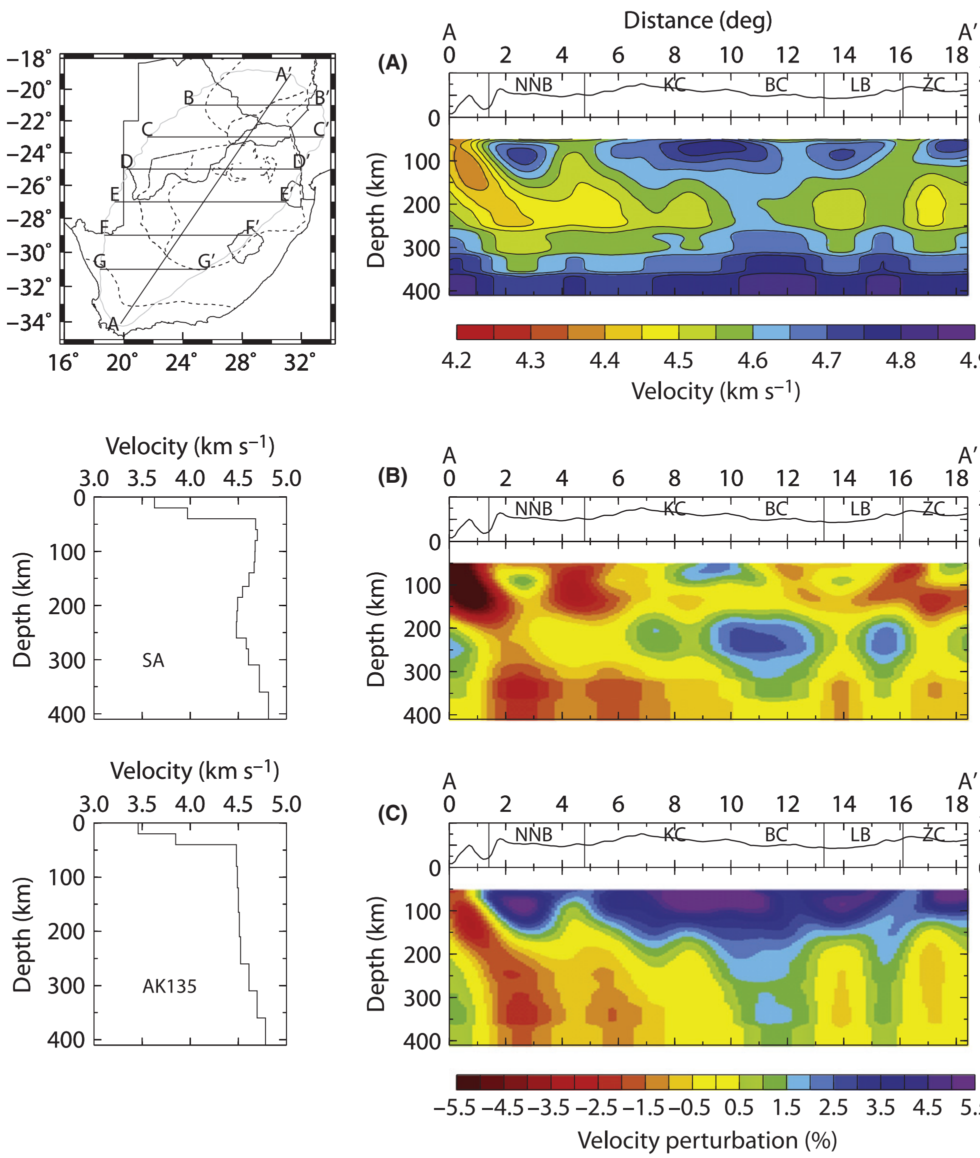

Fig. 14 Absolute wave speed and wave-speed perturbation profiles across southern Africa. (A) Wave-speed profile along A-A' (map at left). (B) Wave-speed perturbation profile of A-A' relative to the average shear wave speed in southern Africa (left). (C) Wave-speed perturbation profile of A-A' relative to the standard global model AK135 (Kennett *et al.*, 1995; left). Topography is plotted above the wave-speed- and wave-speed-perturbation profiles. Vertical lines indicate tectonic boundaries (from Li and Burke, 2006).

higher if the reference wave-speed model were not provided in a form that facilitates comparison with the cross-section.

But which "average" wave-speed model should be used? Reference models such as PREM (Dziewonski and Anderson, 1981) or AK135 (Kennett *et al.*, 1995) are not unique and depend on the data used to derive them. As oceans comprise 70% of the Earth, PREM is dominated by oceanic structure. Upper-mantle seismic wave-speed structure differs substantially between the oceans and continents, so a single, averaged global model is inappropriate for almost every region.

PREM has an abrupt increase in v_P and v_S at 220 km depth (the Lehmann discontinuity). Gu *et al.* (2001a,b) conclude that it is found preferentially under continents, it is intermittent and variable and it is not global. Recent, three-dimensional models of v_S show that what is expressed as a step in PREM may be a rapid decrease in lateral heterogeneity between 200 and 300 km (Thybo and Perchuc, 1997; Thybo, 2006; Cammarano and Romanowicz, 2007; Kustowski *et al.*, 2008; Deuss, 2009). This feature is not necessarily global, however.

The Lehmann discontinuity is inherited by all tomographic models that are calculated using PREM as a starting model. Thus, the wave-speed reductions and strong gradients

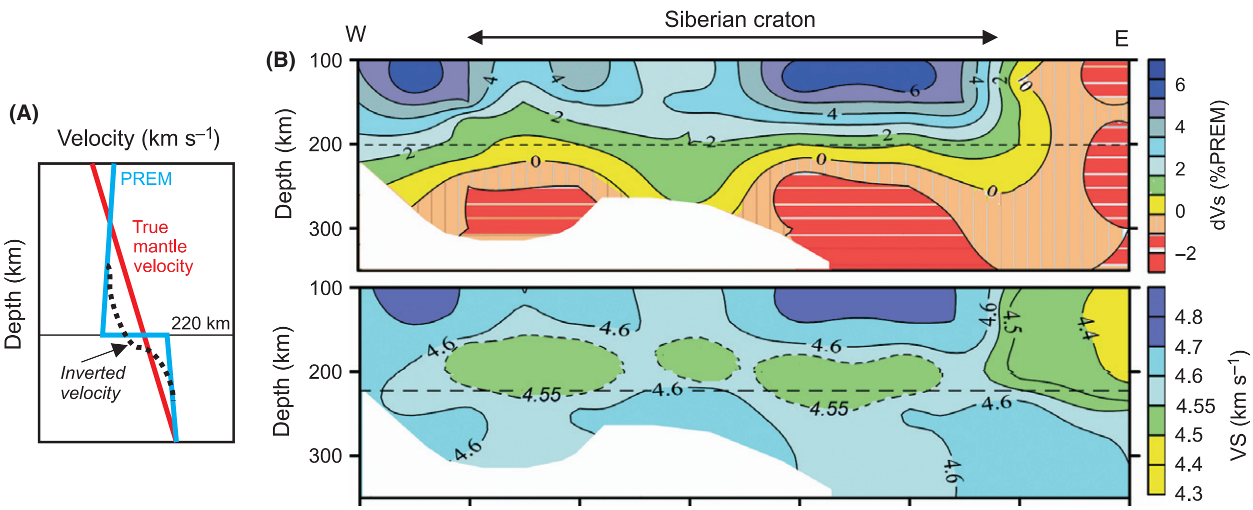

Fig. 15 Using PREM (Dziewonski and Anderson, 1981) as a reference model in tomographic inversions for continental regions may lead to erroneous interpretations of the thickness of the seismic lithosphere (after Artemieva, 2011). (A) Sketch illustrating how the inversion result (dashed line) tends to 'smooth' the step at 220 km depth (a step not required for the continental mantle) by increasing wave speeds above, and decreasing wave speeds below, 220 km depth. This artificially enhances the velocity gradient across 220 km depth. Nonetheless, wave speeds still remain lower than true mantle wave speeds above 220 km and higher below. (B, C) Wave-speed structure of the upper mantle beneath Siberia. Top: Relative v_S perturbations with respect to PREM based on Rayleigh-wave tomography and interpreted as evidence of a 200-km-thick lithosphere beneath the Siberian craton (Priestley and Debayle, 2003). Bottom: the same wave-speed model recalculated to absolute velocities provides no evidence for the base of the lithosphere above 300 km, and it inherits from PREM the reduced wave-speed layer above 220 km (Artemieva, 2011).

commonly observed in derived models at ~220 km depth may be artefacts (Thybo, 2006). Nevertheless, many authors have concluded from inversion results that in stable continental regions, the lithosphere-asthenosphere boundary is at ~220 km depth, whereas such an inversion feature at this depth was made inevitable by the original starting model used.

The question of what is an appropriate reference model is particularly important in the case of subduction zones. If the starting model LVZ wave speeds are too high, the imaged slab will appear to be broken. Artificial slab detachments appear in images of the Apennine, Zagros, Hellenides, Andine and Farallon slabs. Tomographic cross-sections of the Aegean typically reveal a false discontinuity in the slab at 100–150 km depth (Agostini *et al.*, 2010). Displaying tomographic results for the Mediterranean region is problematic because of strong lateral heterogeneity there. A study volume may contain both continental and oceanic subducted lithosphere because a complex of passive continental margins inherited from the Tethys Ocean was subducted (e.g. Handy *et al.*, 2010; Carminati *et al.*, 2012). Some subducted material may even have wave speeds lower than those of the hosting mantle. Under these conditions, a realistic geological structure cannot be illustrated using a single one-dimensional reference model, and three-dimensional starting models need to be used. Misleading images parse into interpretations, e.g. in the apparent misalignment between shallow, subduction-related earthquakes and the high-wave-speed zone inferred to be the subducted slab (Agostini *et al.*, 2010).

Methods do nevertheless exist for retrieving absolute wave speeds, and not just perturbations to a starting model (e.g. Cammarano *et al.*, 2003; Katzman *et al.*, 1998; Levshin *et al.*, 2007; Panza *et al.*, 2010; Ritzwoller *et al.*, 2002; Shapiro and Ritzwoller, 2002; Thybo, 2006; Yang *et al.*, 2007; Yanovskaya and Kozhevnikov, 2003; http://ciei.colorado.edu/˜nshapiro/MODEL/). The best absolute models use all available data, including, for example, local and regional earthquakes and artificial sources, which introduce turning waves (e.g. Du and Panza, 1999; Panza *et al.*, 2007; Anderson, 2011; Brandmayr *et al.*, 2011). These are superior to models based on adding calculated anomalies to starting models.

Displaying the results

Published tomographic maps and cross-sections may give very different impressions, depending on the design choices made:

1 Regions where there are no sampling rays are commonly filled with the "zero anomaly" colour corresponding to no perturbation to the initial starting model. They are thus indistinguishable from well-sampled regions where a wave speed similar to that of the initial model was robustly determined (Section "Inhomogeneous ray coverage"). Such use of colour can give the visual impression that an anomalous region, well-resolved because it lies beneath the centre of the network, is embedded in extensive volumes of "normal" background structure.
2 Vertical exaggeration can make short, broad bodies appear to be tall and chimney-like (Fig. 16).
3 Where bodies are complex and three-dimensional, cross-sections

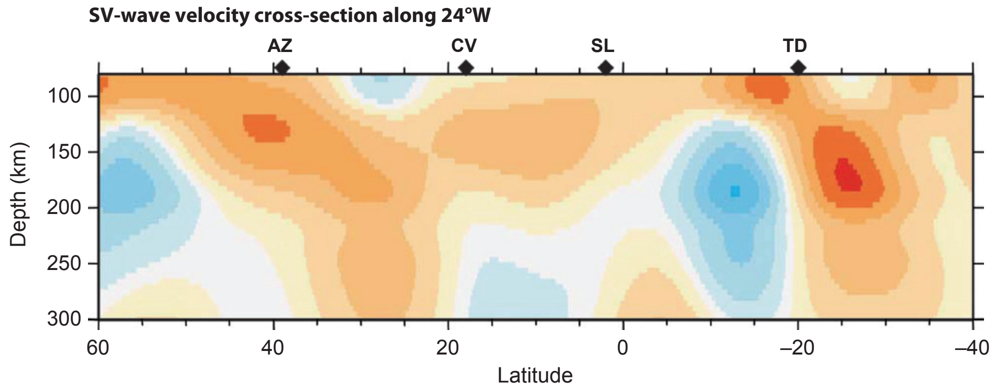

Fig. 16 Cross-section of mantle v_S structure from surface-wave tomography, along longitude 24°W, passing close to the Azores, Cape Verde, Sierra Leone and Tristan da Cunha. The vertical exaggeration of 14 makes quasi-horizontal regions of low seismic wave-speed appear to be quasi-vertical (from Silveira and Stutzmann, 2002).

varying in orientation by only a few degrees, or by short distances laterally, can give very different visual impressions. Truncation of cross-sections can conceal adjacent anomalies at odds with the preferred interpretation (Fig. 17).

4 Very different impressions may be given, depending on the choice of colour scales, and by using different scales for different parts of the imaged volume. Anomalies imaged in the lower mantle are generally much weaker than those imaged in the upper mantle. Despite this, figures can be made to give the impression that uniform structures traverse the entire mantle by using a colour scale that saturates at a fraction of the maximum upper-mantle anomaly (Fig. 17), or by using different colour scales for upper- and lower-mantle regions. An example of the latter is a recent study by Wolfe *et al.* (2009), in which the colour scale used saturates at ± 4% for anomalies at 100 km depth, ± 2% for anomalies at 300 and 400 km, and at ± 1% for anomalies at 600, 900

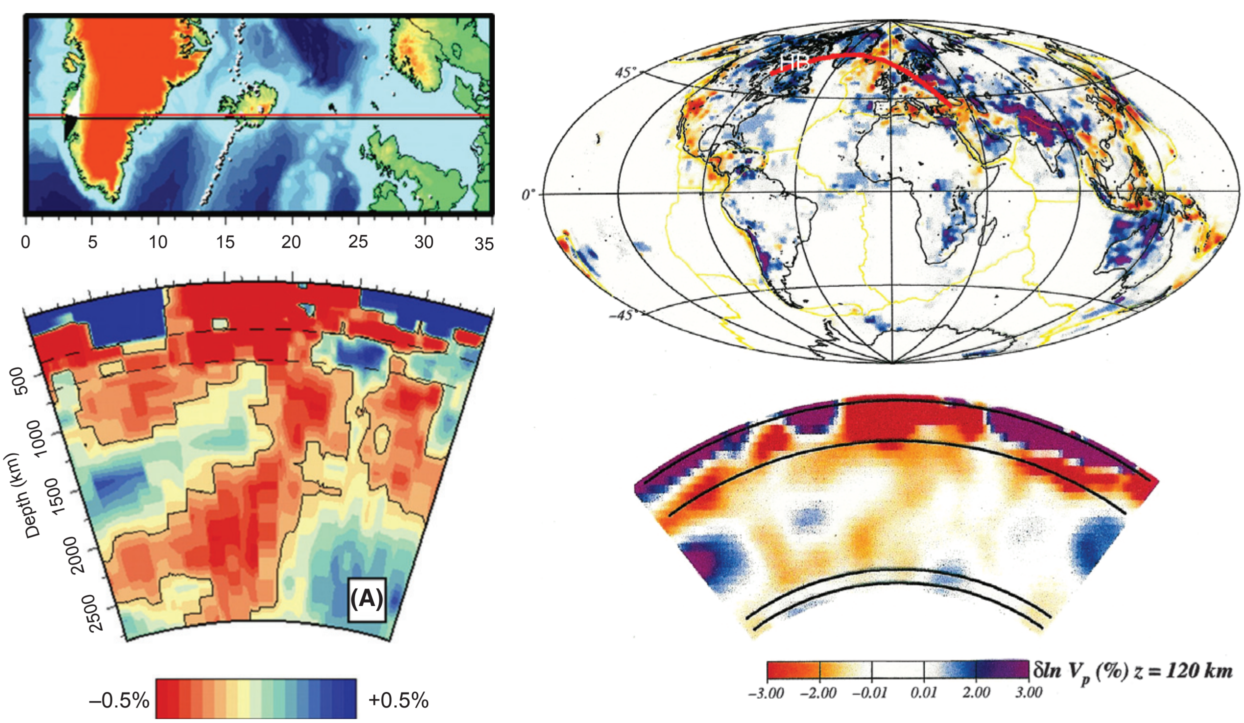

Fig. 17 Left: whole-mantle tomography model. The cross-section shown in (a) purports to show a mantle plume extending from the surface down to the core-mantle boundary under the North Atlantic (from Bijwaard and Spakman, 1999). Right: The same model, re-plotted with the colour scale saturated at an anomaly strength of ± 3%, and the line of section extended to underlie Canada and Scandinavia. HB: Hudson Bay. In the figure at left, saturation of the colour scale at ± 0.5% gives the impression that a low wave-speed structure of roughly constant strength traverses the entire mantle, and truncation of the section at Greenland conceals the very similar structure imaged beneath Hudson Bay.

and 1200 km. A cross-section using a colour scale throughout that saturates near to the upper-mantle maximum anomalies reveals the true picture, which is that an entirely different, weak, downward-continuing anomaly underlies a much stronger, shallow anomaly that does not extend deeper than 400–500 km (Fig. 8, right). Saturating the colour scale at very low anomaly amplitudes can impart the visual impression of significance to weak anomalies that are simply noise, i.e. unresolved.

Translating the results to other physical variables

It is common interpretive practice to assume that red and blue colours (low and high wave speeds) correspond directly to "hot" and "cold" volumes (e.g. VanDecar *et al*., 1995; Faccenna and Beker, 2010). For example, low relative wave speeds beneath the British Isles have been used to argue for hot, partially molten plume material with a temperature anomaly of ~200 °C (Arrowsmith *et al*., 2005; Wawerzinek *et al*., 2008). Low relative wave speeds below ~200 km under the Siberian Craton (Fig. 15) and other stable continents have been ascribed to hot asthenosphere (McKenzie and Priestley, 2008). Many such interpretations are inappropriate because the apparent low wave speeds are not low relative to the global mean (Section "Absolute and relative wave speeds") (Poupinet, 1979; Poupinet *et al*., 2003; Pilidou *et al*., 2004, 2005; Amaru *et al*., 2008).

In particular for local- and regional-scale structures, ambiguity in the physical interpretation of anomalies is commonly ignored, even in geologically complex areas. The amplitudes of seismic anomalies in published teleseismic tomography maps and cross-sections cannot be used meaningfully to constrain geological models or to estimate temperature, composition or degree of partial melt because calculated amplitudes are subjective (Section "Anomaly amplitudes cannot be reliably determined"). Even when no correlation is observed between heat flow and temperature calculated using teleseismic tomography anomalies, the latter are still commonly interpreted solely in terms of temperature (Goes *et al*., 2000; Faccenna and Beker, 2010).

Teleseismic tomography studies typically measure only v_P and v_S, but given the difficulty in determining anomaly amplitude reliably (Section "Anomaly amplitudes cannot be reliably determined"), it is generally not possible to deduce unambiguously the physical explanations for observed wave-speed variations.

Long-wavelength variations in global upper-mantle seismic models are mostly due to temperature (Cammarano *et al*., 2011). However, on local and regional scales, mineralogical and chemical heterogeneities, as well as partial melt, crystal size and the presence of hydrogen and carbon may have greater effects than temperature on seismic wave speed and cannot be ignored (Table 1). The presence of melt strongly lowers wave speed (Murase and Kushiro, 1979; Murase and Fukuyama, 1980; Schmeling, 1985; Hier-Majumder and Courtier, 2011). The wave-speed reduction in v_P and v_S corresponding to a temperature increase of ~100 °C can equally well be caused by the presence of < 0.5% of partial-melt, or very small, unconnected grain-boundary melt fractions (Faul and Jackson, 2007). A reduction of ~2% in the forsterite content [Mg/(Mg + Fe)]# in mantle olivine can bring about similar wave-speed reductions (Jordan, 1979; Chen, 1996; Chen *et al*., 1996; Artemieva, 2009; Cammarano *et al*., 2011).

In a very few, exceptional cases, the physical explanation for seismic anomalies can be deduced. The most notable is the case of the Large Low-Shear-Velocity Provinces (LLSVPs–also known as "superplumes"). These are two vast regions of low v_S in the lower mantle beneath much of the southern Pacific Ocean and the southern Atlantic Ocean-South Africa-southwest Indian Ocean. It is widely assumed that they owe their low wave speeds to high temperature, and popular geodynamic interpretations assume this (e.g. Courtillot *et al*., 2003). It has, however, been shown using normal modes that they owe their low wave speeds to compositional variations and that they have relatively high densities and approximately normal temperatures (Ishii and Tromp, 2004; Trampert *et al*., 2004; Trampert and van der Hilst, 2005). They are thus not buoyant or rising.

A further example of a low wave-speed body that is not hot underlies the Ontong Java Plateau, extending from the near-surface down to ~300 km depth with v_S up to 5% lower than the global average. A study of seismic *ScS* phases (shear waves reflected off the core) reveals that attenuation within the body is low compared with the rest of the

Table 1 Typical reductions in v_P and v_S for plausible variations in composition, degree of partial melt and temperature in the mantle. T_m: solidus temperature.

Phase	Partial melt (per 1% increase in melt content)*	Composition (per 4% reduction in Mg# = Mg/(Mg + Fe) in olivine)**	Temperature (per 100 K increase)*** $T < 0.8\ T_m$	Temperature (per 100 K increase)* $0.8\ T_m < T < 1.1\ T_m$
v_P	1–3%	7%	1%	up to 10%
v_S	3–10%	12%	1.5%	up to 10%

*Depends critically on melt geometry. Numbers in the table refer to laboratory experiments. A significant shear wave velocity decrease, such as observed in the LVZ, can be produced by very small, unconnected grain boundary melt fractions (Murase *et al*., 1977; Murase and Kushiro, 1979; Mavko, 1980; Murase and Fukuyama, 1980; Schmeling, 1985; Faul and Jackson, 2007).

**Numbers in the table account for compositional variations in iron-content only. Other compositional and mineralogical effects may also be influential. For example, in cratonic roots, iron depletion is often correlated with orthopyroxene-depletion, which may have the opposite effects on seismic velocities. This may cancel out, or even reverse the effect of iron depletion (Jordan, 1979; Lee, 2003; Artemieva, 2011).

***(Kern, 1978; Sumino and Anderson, 1982).

Pacific mantle (Gomer and Okal, 2003). The combination of low-v_S and low attenuation rules out temperature alone as the cause of the anomaly and requires a high-viscosity, chemical interpretation (Klosko *et al*., 2001).

Corresponding examples of high wave-speed materials that are not dense or sinking are harzburgite and clinopyroxene-poor lherzolite. These are buoyant because the Fe-Mg solid solution minerals olivine and pyroxene are Fe-poorer than primitive (i.e. not subject to previous basaltic melt extraction) mantle compositions. A suite of global and regional studies have shown that, as a general rule, the effects of temperature and composition on buoyancy are comparable in the shallow continental mantle (Jordan, 1975; Forte and Perry, 2000; Kaban *et al*., 2003; Kelly *et al*., 2003; Artemieva, 2007; Brandmayr *et al*., 2011; Tumanian *et al*., 2012). In the deep mantle, composition and not temperature dominates buoyancy (Trampert and van der Hilst, 2005).

Implications for the geochemical and geodynamic models of the mantle

Acceptance of non-unique interpretations of tomographic images has led to geological and geodynamic models that are not required by the data. These include proposals that the British Isles are underlain by hot plume material (e.g. Arrowsmith *et al*., 2005; Wawerzinek *et al*., 2008), that plumes underlie several islands in the Indian Ocean (Montelli *et al*., 2004a,b), that a plume feeding Hawaii is rooted variously to the NW, or the SE of the Big Island (Li *et al*., 2008; Wolfe *et al*., 2009), and that sodic alkaline-to-tholeiitic continental and oceanic mid-plate magmatism requires thermal anomalies (Ritter *et al*., 2001; Piromallo *et al*., 2008). The assumption that low seismic wave speeds indicate hot material has led to proposals that sub-lithospheric channels up to thousands of kilometres long connect volcanic regions thought to have similar geochemical signatures (e.g. Gibson *et al*., 1995; Oyarzun, 1997; Niu *et al*., 1999; Piromallo *et al*., 2008; Duggen *et al*., 2009).

East African Rift volcanism has been widely attributed to the "African superplume", while the absence of volumetrically relevant igneous activity in southern Africa over the last 180 Ma has been de-emphasized. The latter is consistent with the LLSVPs not being hot (e.g. Bailey, 1992; Pik *et al*., 2006). The exotic magmas of the East African Rift system suggest a compositionally anomalous underlying shallow mantle (e.g. Boven *et al*., 1998; Tappe *et al*., 2003; Bailey and Woolley, 2005; Furman, 2007; Eby *et al*., 2009; Muravyeva and Senin, 2009; Rosenthal *et al*., 2009). An explanation for the volcanism rooted in shallow source compositional heterogeneity is more likely than lower-mantle temperature excess.

In addition to local studies, tomography images that are sometimes invalid are widely used by geochemists to support geochemical models of the entire mantle. Conversely, evidence from geochemistry is often cited in support of interpretations of seismic tomography images. This is sometimes equally invalid because interpretations of geochemical data also suffer from problems and ambiguities.

It cannot be assumed that high wave-speed parts of the core-mantle boundary region are "slab graveyards", and that the LLSVPs are hot and buoyant. Together, these two assumptions underpin whole-mantle convection models that attribute the geochemical signature of ocean-island basalts to the sweeping up of subducted crust in deep-mantle plumes. This, in turn, has bolstered models that attribute geochemical species such as high-$^{3}He/^{4}He$ to the deep lower mantle, and view the core-mantle boundary as the only mantle region where significant radiogenic growth can occur (e.g. ^{206}Pb from ^{238}U; Hofmann, 1988, 1997, 2003; White, 2010). Interestingly, the highest $^{3}He/^{4}He$ measured in terrestrial basalts (~50 times the atmospheric $^{3}He/^{4}He$ ratio; Stuart *et al*., 2003) is associated with extremely high $^{143}Nd/^{144}Nd$ (0.51284–0.5135) and low $^{87}Sr/^{86}Sr$ (0.7030–0.7039) isotopic ratios, as well as low-to-very-low incompatible element contents (e.g. La/Lu normalized to CI chondrite estimate < 1; Jackson *et al*., 2010). All these features indicate a depleted, not an undegassed/undepleted/primitive, mantle source.

It has been surmised that the remaining 99% of the mantle is too cold relative to its solidus temperature to melt, that it is homogenized by convection, and that regions of daughter-isotope accumulation cannot exist within it (e.g. Cadoux *et al*., 2007). As a result, it has been suggested that the upper mantle can only produce melts at mid-ocean ridges by passive adiabatic upwelling, and that igneous rocks with major- and trace-element compositions different from normal mid-ocean ridge basalt (NMORB) involve a separate, deep-mantle source (White, 2010; Farnetani *et al*., 2012; Webber *et al*., 2013; Zhou and Dick, 2013).

From a geochemical point of view, the isotopic compositions of all oceanic-island- and ridge basalts, as well as nearly all mid-plate continental basalts (away from active or fossil subduction zones), can be wrapped in a four-apex polyhedron the end-members of which have been labelled HIMU (High-μ, where $\mu = {}^{238}U/{}^{204}Pb$ ratio), EMI (Enriched Mantle type I), EMII (Enriched Mantle type II) and DMM (Depleted MORB Mantle; Zindler and Hart, 1986). A fifth, very common component (FOZO = Focus Zone) shows intermediate Sr-Nd-Pb-Hf isotope characteristics (Hofmann, 2003; Stracke *et al*., 2005; White, 2010; Stracke, 2012). Isotopic similarities of oceanic or continental mid-plate magmas to one or more of HIMU, EMI and EMII are commonly considered to be proof of a deep-mantle source origin (Hofmann, 2003; White, 2010). However, there is no geochemical or petrological requirement for this. Although a unifying geochemical-petrological theory for how the mantle works is still lacking, there are three generally accepted conclusions:

1. The radiogenic and stable isotopic ratios of mid-ocean ridge and mid-plate magmas can be explained only by invoking the presence of recycled crust and/or shallow lithospheric-mantle and/or reactive products between high-pressure melts and ambient mantle matrix;
2. The upper mantle is heterogeneous from crystal to continental scales and

3 No unambiguous evidence for mass transfer from the Earth's core has been demonstrated (e.g. Scherstén *et al*., 2004; Stracke *et al*., 2005; Anderson, 2011; Lustrino, 2011; Stracke, 2012).

Any tomographic image used to argue for hot or deep-mantle sources cannot, therefore, be verified by geochemical observations – no geochemical observations require a deep-mantle origin.

There are, nevertheless, examples where seismic and petrological data comprise a useful mutual support pair. A steep decrease in the carbonated peridotite solidus of 400–500 °C occurs at ~2 GPa (~60 km), approximately coinciding with the top of the LVZ under oceans. This suggests that this layer contains partial melt (e.g. Wyllie, 1988; Presnall and Gudmundsson, 2011). The top of the LVZ also corresponds to the depth at which the pargasitic amphibole, the main water-storage mineral in the shallow mantle at average geotherms, becomes unstable. At this depth (~90–110 km), the water-storage capacity of mantle peridotite drops from ~0.3 to 0.4 wt% to a few hundred ppm (Mierdel *et al*., 2007; Green *et al*., 2010). As a result, partial melting of lithospheric mantle may onset at the wet solidus (Thybo and Perchuc, 1997), several hundred degrees C cooler than the water-undersaturated solidus (Green *et al*., 2010). The presence of small amounts of hydrous basaltic melts at these depths is also in agreement with the enhanced electric conductivity of the LVZ (Ádám and Panza, 1989; Ni *et al*., 2011).

Summary

Problems with travel-time tomography include inadequate correction for structure outside the study volume, inability to retrieve three-dimensional structure, corruption of the mantle image by inadequate correction of the crust and boundary layer beneath, inability to retrieve true anomaly amplitudes and inhomogeneous ray coverage. Some regions simply cannot be imaged using current techniques, particularly in remote oceanic regions. Perhaps the most vexed problem is assessing realistically the true errors in results. Because of the fundamental experimental set-up, errors in structures calculated using teleseismic tomography are largest in the vertical direction. This results in a propensity to downward-smear structures, producing artificially vertically elongated anomalies. For surface-wave tomography, lateral resolution of anomalies is poorest and therefore lateral smearing can be strong.

The information in three-dimensional models is difficult to impart in a few maps and cross-sections. The wide array of choices, such as which particular result to favour, and which colour palette, line of section, and zero-contour wave speed to select, means that there is broad scope for producing figures that support preferred models. The widespread use of relative wave speeds commonly leads to misinterpretations. Translation of seismic anomalies to geology is not straightforward. More physical parameters vary in the mantle than seismic parameters mapped. Simplifying assumptions, such as seismic wave speed being everywhere a direct proxy for temperature, are not supported, and neither are geochemical models that rely on such work.

We have not discussed in depth the issue of anisotropy, and yet this effect may also be profound. The wave speeds of both compressional and shear-waves are anisotropic in the mantle, and if this is neglected, which is usually the case, erroneous results and interpretations may result. Important targets for surface-wave tomography are determining upper-mantle radial anisotropy, and azimuthal and vertical variations in wave speed (Anderson, 1965; Nakanishi and Anderson, 1984; Nataf *et al*., 1984; Tanimoto and Anderson, 1984; Lévêque *et al*., 1998; Gung *et al*., 2003; Kustowski *et al*., 2008). The upper 200 km of the mantle is the most heterogeneous and anisotropic region of the mantle and beneath this, heterogeneity drops dramatically (Gung *et al*., 2003). Many weak anomalies imaged by seismic tomography may result simply from uncorrected anisotropy. Anisotropy at ~200 km beneath cratons and at ~80–200 km beneath ocean basins may be related to shear in the boundary layer, the difference in depth simply reflecting a variable depth to the maximum shear (Anderson, 2011).

In recent years, much progress has been made in improving computational techniques and incorporating these advances into tomographic practice. This includes using local structure in global parameterizations, and three-dimensional ray-tracing instead of assuming straight or piecewise-straight rays (Hung *et al*., 2001, 2004). Similarly, Christoffersson and Husebye (2011) have revisited the basics of the inversion methods used, showing that at least some of the often-noted smearing and weakening of velocity anomalies by traditional damped inverses can be mitigated by using better tuned methods. Progress is also being made on describing better the uncertainties in the results, including calculating probability density functions (Mosegaard and Tarantola, 2002; Sambridge, 1999a,b). However, these advances cannot eliminate the fundamental difficulties we have highlighted above, which are inherent in the experimental setup. There is, nevertheless, a good case for re-processing many older data sets that have only been analysed using earlier, more primitive methods, the results of which continue to influence dynamic models of the mantle.

What is the way forward? Entire digital models, with errors, can now be published on the internet, along with tools to enable authors to make their own plots and cross-sections (Li *et al*., 2008, http://www.earth.lsa.umich.edu/˜jritsema/Research.html). Other seismic results that do not depend on tomography should be included in interpretations, and interpretive work should emphasize only the deductions that are required by the data. Published, coloured tomography images and simplistic, cartoon-like interpretations should be treated with scepticism. Blue colours in tomographic cross-sections cannot be assumed to indicate cold, sinking material and red cannot be assumed to indicate hot, rising material. Likewise, increased awareness is needed that petrology/geochemistry cannot, in general, determine the depth of origin of magma sources. As a consequence, joint interpretation is more difficult than commonly realized. A more cautious approach will enable the current, unprecedented experimental tools available in both seismology and petrology/geochemistry to contribute reliably to answering the fundamental questions about the structure and dynamics of the Earth's interior that have been disputed ever since plate tectonics was accepted and still remain controversial.

Acknowledgements

We thank Adam Dziewonski, Rob van der Hilst, Jeroen Ritsema, Don Anderson and an anonymous reviewer for helpful comments on the draft manuscripts. GFP thanks Progetto Quadro Regione Friuli Venezia Giulia "Definition of seismic and tsunami hazard scenarios by means of Indo-European e-infrastructures", and the Italian PNRA and PRIN for partial financial support of the research that led to some of the results discussed in this article. IMA acknowledges research grant FNU-31402. ML acknowledges grants AST 2008, 2009, Ateneo 2010, 2011 and MIUR-PRIN 2008 (Grant no. 2008HM HYFP_005).

References

Achauer, U., Maguire, P.K.H., Mechie, J., Green, W.V. and group, t.K.w., 1992. Some remarks on the structure and geodynamics of the Kenya rift. *Tectonophysics*, **213**, 257–268.

Ádám, A. and Panza, G.F., 1989. A critical review of the magnetotelluric information on the upper mantle. *Acta Geod. Geoph. Mont. Hung.*, **24**, 395–415.

Agostini, S., Doglioni, C., Innocenti, F., Manetti, P. and Tonarini, S., 2010. On the geodynamics of the Aegean rift. *Tectonophysics*, **488**, 7–21.

Aki, K. and Richards, P.G., 2002. *Quantitative Seismology*. University Science Books, Sausalito, California.

Aki, K., Christoffersson, A. and Husebye, E., 1977. Determination of the three-dimensional seismic structure of the lithosphere. *J. Geophys. Res.*, **82**, 277–296.

Alinaghi, A., Koulakov, I. and Thybo, H., 2007. Seismic tomographic imaging of P- and S-waves velocity perturbations in the upper mantle beneath Iran. *Geophys. J. Int.*, **169**, 1089–1102.

Amaru, M., Spakman, W., Villasenor, A., Sandoval, S. and Kissling, E., 2008. A new absolute arrival time data set for Europe. *Geophys. J. Int.*, **173**, 465–472.

Anderson, D.L., 1965. Recent evidence concerning the structure and composition of the Earth's mantle. In: *Physics and Chemistry of the Earth*, vol. 6 (L.H. Ahrens, J.B. Dawson, S.K. Runcorn and H.C. Urey, eds). Pergamon Press, Oxford.

Anderson, D.L., 1967. Phase changes in the upper mantle. *Science*, **157**, 1165–1173.

Anderson, D.L., 2007. *New Theory of the Earth*. Cambridge University Press, Cambridge.

Anderson, D.L., 2011. Hawaii, boundary layers and ambient mantle–geophysical constraints. *J. Petrol.*, **52**, 1547–1577.

Arrowsmith, S., Kendall, J.-M., White, N. and VanDecar, J., 2005. Seismic imaging of a hot upwelling beneath the British Isles. *Geology*, **33**, 345–348.

Artemieva, I.M., 2007. Dynamic topography of the East European Craton: shedding light upon the lithospheric structure, composition and mantle dynamics. *Global Planet. Change*, **58**, 411–434.

Artemieva, I.M., 2009. The continental lithosphere: reconciling thermal, seismic, and petrologic data. *Lithos*, **109**, 23–46.

Artemieva, I.M., 2011. *The Lithosphere: An Interdisciplinary Approach*. Cambridge Univ. Press, Cambridge.

Backus, G.E. and Gilbert, F., 1967. Numerical applications of a formalism for geophysical inverse problems. *Geophys. J. Roy. Astron. Soc.*, **13**, 247–276.

Backus, G.E. and Gilbert, F., 1968. The resolving power of gross earth data. *Geophys. J. Roy. Astron. Soc.*, **16**, 169–205.

Backus, G. and Gilbert, F., 1970. Uniqueness in the inversion of gross Earth data. *Phil. Trans. Royal Soc. London*, **A266**, 123–192.

Bailey, D.K., 1992. Episodic alkaline igneous activity across Africa. *Magmatism and the Causes of Continental Breakup*, vol. **68** (B.C. Storey, T. Alabaster, R.J. Pankhurst, eds), pp. 91–98. Geological Society, London.

Bailey, D.K. and Woolley, A.R., 2005. Repeated, synchronous magmatism within Africa: timing, magnetic reversals and global tectonics. In: *Plates, Plumes & Paradigms* (G.R. Foulger, J.H. Natland, D.C. Presnall and D.L. Anderson, eds). Geological Society of America, Boulder, Colorado.

Bassin, C., Laske, G. and Masters, G., 2000. The current limits of resolution for surface wave tomography in North America. *EOS Trans, AGU*, **81**, F897.

Bastow, I.D., 2012. Relative arrival-time upper-mantle tomography and the elusive background mean. *Geophys. J. Int.*, **190**, 1271–1278.

Bastow, I.D., Stuart, G.W., Kendall, J.-M. and Ebinger, C.J., 2005. Upper-mantle seismic structure in a region of incipient continental breakup: northern Ethiopian rift. *Geophys. J. Int.*, **162**, 479–493.

Bastow, I.D., Nyblade, A.A., Stuart, G.W., Rooney, T. and Benoit, M.H., 2008. Upper mantle seismic structure beneath the ethiopian hotspot: rifting at the edge of the African low velocity anomaly. *Geochem. Geophys. Geosyst.*, **9**, doi:10.1029/2008GC002107.

Becker, T.W., 2012. On recent seismic tomography for the western United States. *Geochem. Geophys. Geosyst.*, **13**, doi:10.1029/2011GC003977.

Bijwaard, H. and Spakman, W., 1999. Tomographic evidence for a narrow whole mantle plume below Iceland. *EPSL*, **166**, 121–126.

Billien, M., Lévêque, J.-J. and Trampert, J., 2000. Global maps of Rayleigh wave attenuation for periods between 40 and 150 seconds. *Geophys. Res. Lett.*, **27**, 3619–3622.

Bonatti, E., 1990. Not so hot "hot spots" in the oceanic mantle. *Science*, **250**, 107–111.

Boschi, L. and Ekstrom, G., 2002. New images of the upper mantle from measurements of surface wave phase velocity anomalies. *J. Geophys. Res.*, **107**, doi:10.1029/2000JB000059.

Boven, A., Pasteels, P., Punzalan, L.E., Yamba, T.K. and Musisi, J.H., 1998. Quaternary perpotassic magmatism in Uganda (Toro-Ankole volcanic Province): age assessment and significance for magmatic evolution along the East African Rift. *J. Afr. Earth Sci.*, **26**, 463–476.

Boyadzhiev, G., Brandmayr, E., Pinat, T. and Panza, G.F., 2008. Optimization for non-linear inverse problems. *Rendiconti Lincei*, **19**, 17–43.

Brandmayr, E., Raykova, R., Zuri, M., Romanelli, F., Doglioni, C. and Panza, G.F., 2010. The lithosphere in Italy: structure and seismicity. In: *The Geology of Italy* (M. Beltrando, A. Peccerillo, M. Mattei, S. Conticelli and C. Doglioni, eds). *J Virtual Explorer*, **36**, 1.

Brandmayr, E., Marson, I., Romanelli, F. and Panza, G.F., 2011. Lithosphere density model in Italy: no hint for slab pull. *Terra Nova*, **23**, 292–299.

Bruneton, M., Pedersen, H.A., Vacher, P., Kukkonen, I.T., Arndt, N.T., Funke, S., Friederich, W. and Farra, V., 2004. Layered lithospheric mantle in the central Baltic Shield from surface waves and xenolith analysis. *Earth Planet. Sci. Lett.*, **226**, 41–52.

Cadoux, A., Blichert-Toft, J., Pinti, D.L. and Albarède, F., 2007. A unique lower mantle source for Southern Italy volcanics. *Earth Planet. Sci. Lett.*, **259**, 227–238.

Cammarano, F. and Romanowicz, B., 2007. Insights into the nature of the transition zone from physically constrained inversion of long period seismic data. *PNAS-High Press. Geosci*., **104**, 9139–9144.

Cammarano, F., Goes, S., Vacher, P. and Giardini, D., 2003. Inferring upper mantle temperatures from seismic velocities. *Phys. Earth Planet. Inter*., **138**, 197–222.

Cammarano, F., Tackley, P. and Boschi, L., 2011. Seismic, petrological and geodynamical constraints on thermal and compositional structure of the upper mantle: global thermo-chemical models. *Geophys. J. Int*., **187**, 1301–1318.

Cara, M., 1979. Lateral variations of S-velocity in the upper mantle from higher Rayleigh modes. *Geophys. J. Roy. Astron. Soc*., **5**, 649–670.

Carminati, E. and Doglioni, C., 2010. North Atlantic geoid high, volcanism and glaciations. *Geophys. Res. Lett*., **37**, doi:10.1029/2009GL041663.

Carminati, E., Lustrino, M. and Doglioni, C., 2012. Geodynamic evolution of the central and western Mediterranean: Tectonics vs. igneous petrology constraints. *Tectonophysics*, **579**, 173–192.

Chen, Y.D., 1996. Constraints on melt production rate beneath the mid-ocean ridges based on passive flow models. *Pure Appl. Geophys*., **146**, 589–620.

Chen, G., Spetzler, H.A., Gettinag, I.C. and Yoneda, A., 1996. Selected elastic moduli and their temperature derivatives for olivine and garnet with different Mg/(Mg+Fe) contents: Results from GHz ultrasonic interferometry. *Geophys. Res. Lett*., **23**, 5–8.

Christoffersson, A. and Husebye, E.S., 2011. Seismic tomographic mapping of the Earth's interior — Back to basics revisiting the ACH inversion. *Earth Sci. Rev*., **106**, 293–306.

Corchete, V. and Chourak, M., 2010. Shear-wave velocity structure of the western part of the Mediterranean Sea from Rayleigh-wave analysis. *Int. J. Earth Sci. (Geol. Rundsch.)*, **99**, 955–972.

Corchete, V. and Chourak, M., 2011. Shear-wave velocity structure of the south-eastern part of the Iberian Peninsula from Rayleigh wave analysis. *Int. J. Earth Sci. (Geol. Rundsh.)*, **100**, 1733–1747.

Courtillot, V., Davaillie, A., Besse, J. and Stock, J., 2003. Three distinct types of hotspots in the Earth's mantle. *Earth Planet. Sci. Lett*., **205**, 295–308.

Curtis, A., Trampert, J. and Snieder, R., 1998. Eurasian fundamental mode surface wave phase velocities and their relationship with tectonic structures. *J. Geophys. Res*., **103**, 26919–26947.

Dahlen, F.A. and Tromp, J., 1998. *Theoretical Global Seismology*. Princeton University Press, Princeton, New Jersey.

Dahlen, F.A., Hung, S.-H. and Nolet, G., 2000. Frechet kernels for finite-frequency traveltimes – I. Theory. *Geophys. J. Int*., **141**, 157–174.

Darbyshire, F.A., 2005. Upper mantle structure of Arctic Canada from Rayleigh wave dispersion. *Tectonophysics*, **405**, 1–23.

Davies, J.H. and Bunge, H.-P., 2006. Are splash plumes the origin of minor hotspots? *Geology*, **34**, 349–352.

Deuss, A., 2009. Global Observations of Mantle Discontinuities Using SS and PP Precursors. *Surv. Geophys*., **30**, 301–326.

Doglioni, C., Green, D.H. and Mongelli, F., 2005. On the shallow origin of hotspots and the westward drift of the lithosphere. In: *Plates, Plumes, and Paradigms* (G.R. Foulger, J.H. Natland, D.C. Presnall and D.L. Anderson, eds). Geological Society of America, Boulder, Colorado.

Du, Z. and Panza, G.F., 1999. Amplitude and phase differentiation of synthetic seismograms: a must for waveform inversion at regional scale. *Geophys. J. Int*., **136**, 83–98.

Duggen, S., Hoernle, K.A., Hauff, F., Klugel, A., Bouabdellah, M. and Thirlwall, M.F., 2009. Flow of Canary mantle plume material through a subcontinental lithospheric corridor beneath Africa to the Mediterranean. *Geology*, **37**, 283–286.

Dziewonski, A.M., 1971a. On regional differences in dispersion of mantle Rayleigh waves. *Geophys. J. Roy. Astron. Soc*., **22**, 289–326.

Dziewonski, A.M., 1971b. Upper mantle models from "pure-path" dispersion data. *J. Geophys. Res*., **76**, 2587–2601.

Dziewonski, A.M. and Anderson, D.L., 1981. Preliminary Reference Earth Model. *Phys. Earth Planet. Inter*., **25**, 297–356.

Eby, G.N., Lloyd, F.E. and Woolley, A.R., 2009. Geochemistry and petrogenesis of the Fort Portal, Uganda, extrusive carbonatite. *Lithos*, **113**, 785–800.

Eken, T., Shomali, Z.H., Roberts, R., Hieronymus, C.F. and Bodvarsson, R., 2008. S and P velocity heterogeneities within the upper mantle below the Baltic Shield. *Tectonophysics*, **462**, 109–124.

Ekström, G., Tromp, J. and Larson, E.W.F., 1997. Measurements and global models of surface wave propagation. *J. Geophys. Res*., **102**, 8137–8157.

Ellsworth, W.L., 1977. *Three-dimensional Structure of the Crust and Mantle Beneath the Island of Hawaii*. Ph.D., Massachusetts Institute of Technology, 327 p.

Evans, J.R. and Achauer, U., 1993. Teleseismic velocity tomography using the ACH method: theory and application to continental-scale studies. In: *Seismic Tomography: Theory and Applications* (H.M. Iyer and K. Hirahara, eds). Chapman and Hall, London.

Evans, J.R. and Zucca, J.J., 1993. Active source, high-resolution (NeHT) tomography: velocity and Q. In: *Seismic Tomography: Theory and Applications* (H.M. Iyer and K. Hirahara, eds). Chapman and Hall, London.

Faccenna, C. and Beker, T.W., 2010. Shaping mobile belts by small-scale convection. *Nature*, **465**, 602–605.

Farnetani, C., Hofmann, A.W. and Class, C., 2012. How double volcanic chains sample geochemical anomalies from the lowermost mantle. *Earth Planet. Sci. Lett*., **359-360**, 240–247.

Faul, U.H. and Jackson, I., 2007. Diffusion creep of dry, melt-free olivine. *J. Geophys. Res*., **112**, doi:10.1029/2006JB004586.

Feng, M., Lee, S.v.d. and Assumpcao, M., 2007. Upper mantle structure of South America from joint inversion of waveforms and fundamental mode group velocities of Rayleigh waves. *J. Geophys. Res*., **112**, doi:10.10292006JB004449.

Forte, A.M. and Perry, A.C., 2000. Seismic-geodynamic evidence for a chemically depleted continental tectosphere. *Science*, **290**, 1940–1944.

Foulger, G.R., Miller, A.D., Julian, B.R. and Evans, J.R., 1995. Three-dimensional Vp and Vp/Vs structure of the Hengill triple junction and geothermal area, Iceland, and the repeatability of tomographic inversion. *Geophys. Res. Lett*., **22**, 1309–1312.

Foulger, G.R., Pritchard, M.J., Julian, B.R., Evans, J.R., Allen, R.M., Nolet, G., Morgan, W.J., Bergsson, B.H., Erlendsson, P., Jakobsdottir, S., Ragnarsson, S., Stefansson, R. and Vogfjord, K., 2001. Seismic tomography shows that upwelling beneath Iceland is confined to the upper mantle. *Geophys. J. Int*., **146**, 504–530.

Frederiksen, A.W., Miong, S.-K., Darbyshire, F.A., Eaton, D.W., Rondenay, S. and Sol, S., 2007. Lithospheric variations across the Superior Province, Ontario, Canada: Evidence from tomography and shear wave splitting. *J. Geophys. Res*., **112**, doi:10.1029/2006JB004861.

Furman, T., 2007. Geochemistry of East African Rift basalts: an overview. *J. Afr. Earth Sci.*, **48**, 147–160.
Gibson, S.A., Thompson, R.N., Leonardos, O.H., Dickin, A.P. and Mitchell, J.G., 1995. The Late Cretaceous impact of the Trinidade mantle plume: Evidence from large volume, mafic potassic magmatism in SE Brazil. *J. Petrol.*, **36**, 189–229.
Goes, S., Govers, R. and Vacher, P., 2000. Shallow mantle temperatures under Europe from *P* and *S* wave tomography. *J. Geophys. Res.*, **105**, 11153–111169.
Gomer, B.M. and Okal, E.A., 2003. Multiple-ScS probing of the Ontong-Java Plateau. *Earth Planet. Sci. Lett.*, **138**, 317–331.
Gonzales, O., Alvarez, L., Moreno, B. and Panza, G.F., 2011. S-Wave velocities of the lithosphere-asthenosphere system in the caribbean region. *Pure Appl. Geophys.*, doi:10.007/s00024-011-0321-3.
Grand, S.P., Van Der Hilst, R.D. and Widiyantoro, S., 1997. Global seismic tomography: A snapshot of convection in the Earth. *GSA Today*, **7**, 1–7.
Green, W.V., Achauer, U. and Meyer, R.P., 1991. A 3-Dimensional seismic image of the crust and upper mantle beneath the kenya rift. *Nature*, **354**, 199–203.
Green, D.H., Hibberson, W.O., Kovacs, I. and Rosenthal, A., 2010. Water and its influence on the lithosphere-asthenosphere boundary. *Nature*, **467**, 448–452.
Gregersen, S., Voss, P. and Group, T.W., 2002. Summary of project TOR: delineation of a stepwise, sharp, deep lithosphere transition across Germany-Denmark-Sweden. *Tectonophysics*, **360**, 61–73.
Gu, Y.J., Dziewonski, A.M. and Ekstrom, G., 2001a. Preferential detection of the Lehmann discontinuity beneath continents. *Geophys. Res. Lett.*, **24**, 4655–4658.
Gu, Y.J., Dziewonski, A.M., Weijia, S. and Ekstrom, G., 2001b. Models of the mantle shear velocity and discontinuities in the pattern of lateral heterogeneities. *J. Geophys. Res.*, **106**, 11169–111199.
Gung, Y., Panning, M.P. and Romanowicz, B., 2003. Global anisotropy and the thickness of continents. *Nature*, **422**, 707–711.
Hamilton, W.B., 2007. Driving mechanism and 3-D circulation of plate tectonics. In: *Whence the Mountains? Inquiries into the Evolution of Orogenic Systems: A Volume in Honor of Raymond A. Price* (J.W. Sears, T.A. Harms and C.A. Evenchick, eds). Geological Society of America, Boulder, CO.
Hamilton, W.B., 2011. Plate tectonics began in Neoproterozoic time, and plumes from deep mantle have never operated. *Lithos*, **123**, 1–20.
Handy, M.R., Schmid, S.M., Bousquet, R., Kissling, E. and Bernoulli, D., 2010. Reconciling plate-tectonic reconstructions of Alpine Tethys with the geological–geophysical record of spreading and subduction in the Alps. *Earth Sci. Rev.*, **102**, 121–158.
Hier-Majumder, S. and Courtier, A., 2011. Seismic signature of small melt fraction atop the transition zone. *Earth Planet. Sci. Lett.*, **308**, 334–342.
van der Hilst, R.D. and de Hoop, M.V., 2005. Banana-doughnut kernels and mantle tomography. *Geophys. J. Int.*, **163**, 956–961.
van der Hilst, R., Engdahl, E.R. and Spakman, W., 1993. Tomographic inversion of P and pP data for aspherical mantle structure below the northwest Pacific region. *Geophys. J. Int.*, **115**, 264–302.
Hofmann, A.W., 1988. Chemical differentiation of the Earth: the relationship between mantle, continental crust, and oceanic crust. *Earth Planet. Sci. Lett.*, **90**, 297–314.
Hofmann, A.W., 1997. Mantle geochemistry: the message from oceanic volcanism. *Nature*, **385**, 219–229.
Hofmann, A.W., 2003. Sampling mantle heterogeneity through oceanic basalts: Isotopes and trace elements. In: *Treatise on Geochemistry: The Mantle and Core* (R.W. Carlson, H.D. Holland and K.K. Turekian, eds). Elsevier, Amsterdam.
Hung, S.-H., Dahlen, F.A. and Nolet, G., 2001. Wavefront healing: a banana-doughnut perspective. *Geophys. J. Int.*, **146**, 289–312.
Hung, S.-H., Shen, Y. and Chiao, L.-Y., 2004. Imaging seismic velocity structure beneath the Iceland hotspot: A finite-frequency approach. *J. Geophys. Res.*, **109**, doi:10.1029/2003JB002889.
Ishii, M. and Tromp, J., 2004. Constraining large-scale mantle heterogeneity using mantle and inner-core sensitive normal modes. *Phys. Earth Planet. Inter.*, **146**, 113–124.
Jackson, M.G., Carlson, R.W., Kurz, M.D., Kempton, P.D., Francis, D. and Blusztajn, J., 2010. Evidence for the survival of the oldest terrestrial mantle reservoir. *Nature*, **466**, 853–856.
James, D.E., Niu, F.L. and Rokosky, J., 2003. Crustal structure of the Kaapvaal craton and its significance for early crustal evolution. *Lithos*, **71**, 413–429.
Jordan, T.H., 1975. The continental tectosphere. *Rev. Geophys. Space Phys.*, **13**, 1–13.
Jordan, T.H., 1979. Mineralogies, densities and seismic velocities of garnet lherzolites and their geophysical implications. In: *The Mantle Sample: Inclusions in Kimberlites and Other Volcanics* (F.R. Boyd and H.O.A. Meyer, eds). American Geophysical Union, Washington.
Julian, B.R. and Evans, J.R., 2010. On possible plume-guided seismic waves. *Bull. Seismol. Soc. Am.*, **100**, 497–508.
Kaban, M.K., Schwintzer, P., Artemieva, I.M. and Mooney, W.D., 2003. Density of the continental roots: compositional and thermal effects. *Earth Planet. Sci. Lett.*, **209**, 53–69.
Katzman, R., Zhao, L. and Jordan, T.H., 1998. High-resolution, two-dimensional vertical tomography of the central Pacific mantle using ScS reverberations and frequency-dependent travel times. *J. Geophys. Res.*, **103**, 17933–17971.
Kellogg, L.H. and Wasserburg, G.J., 1990. The role of plumes in mantle helium fluxes. *Earth Planet. Sci. Lett.*, **99**, 276–289.
Kelly, R.K., Kelemen, P.B. and Jull, M., 2003. Buoyancy of the continental upper mantle. *Geochem. Geophys. Geosyst.*, **4**, 1017.
Kennett, B.L.N. and Engdahl, E.R., 1991. Travel times for global earthquake location and phase identification. *Geophys. J. Int.*, **105**, 429–466.
Kennett, B.L.N., Engdahl, E.R. and Buland, R., 1995. Constraints on seismic velocities in the Earth from traveltimes. *Geophys. J. Int.*, **122**, 108–124.
Kern, H., 1978. The effect of high temperature and high confining pressure on compositional wave velocities in quartz-bearing and quartz-free igneous and metamorphic rocks. *Tectonophysics*, **44**, 185–203.
Klosko, E.R., Russo, R.M., Okal, E.A. and Richardson, W.P., 2001. Evidence for a rheologically strong chemical mantle root beneath the Ontong-Java Plateau. *Earth Planet. Sci. Lett.*, **186**, 347–361.
Kustowski, B., Ekström, G. and Dziewonski, A.M., 2008. The shear-wave velocity structure in the upper mantle beneath Eurasia. *Geophys. J. Int.*, **174**, 978–992.
Lebedev, S., Boonen, J. and Trampert, J., 2009. Seismic structure of Precambrian lithosphere: New constraints from broad-band surface-wave dispersion. *Lithos*, **109**, 96–111.
Lee, C.-T.A., 2003. Compositional variation of density and seismic velocities in natural peridotites at STP conditions: Implications for seismic imaging of compositional heterogeneities in the upper mantle. *J. Geophys. Res.*, **108**, 2441, doi:2410.1029/2003JB002413.
van der Lee, S., James, D. and Silver, P., 2001. Upper mantle S velocity structure

of central and western South America. *J. Geophys. Res.*, **106**, 30821–830834.
Legendre, C.P., Meier, T., Lebedev, S., Friederich, W. and Viereck-Gotte, L., 2012. A shear wave velocity model of the European upper mantle from automated inversion of seismic shear and surface waveforms. *Geophys. J. Int.*, **191**, 282–304.
Léveque, J.-J. and Masson, F., 1999. From ACH tomographic models to absolute velocity models. *Geophys. J. Int.*, **137**, 621–629.
Léveque, J.J., Rivera, L. and Wittlinger, G., 1993. On the use of the checker-board test to assess the resolution of tomographic inversions. *Geophys. J. Int.*, **115**, 313–318.
Lévêque, J.J., Debayle, E. and Maupin, V., 1998. Anisotropy in the Indian Ocean upper mantle from Rayleigh- and Love-waveform inversion. *Geophys. J. Int.*, **133**, 529–540.
Levshin, A.L.L., Schweitzer, J., Weidle, C., Shapiro, N. and Ritzwoller, M., 2007. Surface wave tomography of the barents sea and surrounding regions. *Geophys. J. Int.*, **170**, 441–459.
Li, A. and Burke, K., 2006. Upper mantle structure of southern Africa from Rayleigh wave tomography. *J. Geophys. Res.*, **111**, doi:10.1029/2006JB004321.
Li, C., van der Hilst, R.D., Engdahl, E.R. and Burdick, S., 2008. A new global model for P wave speed variations in Earth's mantle. *Geochem. Geophys. Geosyst.*, **9**, doi:10.1029/2007GC001806.
Lippitsch, R., Kissling, E. and Ansorge, J., 2003. Upper mantle structure beneath the Alpine orogen from high-resolution teleseismic tomography. *J. Geophys. Res.*, **108**, doi:10.1029/2002 JB002016.
Lou, X., van der Lee, S. and Lloyd, S., 2013. AIMBAT: A Python/Matplotlib tool for measuring teleseismic arrival times. *Seismol. Res. Lett.*, **84**, 85–93.
Lustrino, M., 2011. What 'anorogenic' igneous rocks can tell us about the chemical composition of the upper mantle: case studies from the circum-Mediterranean area. *Geol. Mag.*, **148**, 304–316.
Marone, F., Gung, Y.C. and Romanowicz, B., 2007. Three-dimensional radial anisotropic structure of the North American upper mantle from inversion of surface waveform data. *Geophys. J. Int.*, **171**, 206–222.
Masson, F. and Trampert, J., 1997. On ACH, or how reliable is regional teleseismic delay time tomography? *Phys. Earth Planet. Inter.*, **102**, 21–32.
Mavko, G.M., 1980. Velocity and attenuation in partially molten rocks. *J. Geophys. Res.*, **85**, 5173–5189.
McKenzie, D. and Priestley, K., 2008. The influence of lithospheric thickness variations on continental evolution. *Lithos*, **102**, 1–11.
Medhus, A.B., Balling, N., Jacobsen, B.H., Weidle, C., England, R.W., Kind, R., Thybo, H. and Voss, P., 2012. Upper-mantle structure beneath the Southern Scandes Mountains and the Northern Tornquist Zone revealed by P-wave traveltime tomography. *Geophys. J. Int.*, **189**, 1315–1334.
Menke, W., 1984. *Geophysical Data Analysis: Discrete Inverse Theory*. Academic Press Inc, Waltham, MA.
Mierdel, K., Keppler, H., Smyth, J.R. and Langenhorst, F., 2007. Water solubility in aluminous orthopyroxene and the origin of Earth's asthenosphere. *Science*, **315**, 354–368.
Montelli, R., Nolet, G., Dahlen, F.A., Masters, G., Engdahl, R.E. and Hung, S.-H., 2004a. Finite frequency tomography reveals a variety of plumes in the mantle. *Science*, **303**, 338–343.
Montelli, R., Nolet, G., Masters, G., Dahlen, F. and Hung, S.-H., 2004b. Global P and PP traveltime tomography: rays versus waves. *Geophys. J. Int.*, **158**, 637–654.
Montelli, R., Nolet, G., Dahlen, F. and Masters, G., 2006. A catalogue of deep mantle plumes: new results from finite-frequency tomography. *Geochem. Geophys. Geosyst.*, doi:11010.11029/12006GC001248.
Mooney, W.D., Laske, G. and Masters, T.G., 1998. CRUST 5.1: A global crustal model at 5° × 5°. *J. Geophys. Res.*, **103**, 727–747.
Mosegaard, K. and Tarantola, A., 2002. Probabilistic Approach to Inverse Problems. In: *International Handbook of Earthquake & Engineering Seismology, Part A*. (William H.K. Lee, P. Jennings, C. Kisslinger and H. Kanamori, eds). Academic Press, London.
Murase, T. and Fukuyama, H., 1980. *Shear Wave Velocity in Partially Molten Peridotite at High Pressures*. Year Book Carnegie Institute, Washington, DC.
Murase, T. and Kushiro, I., 1979. *Compressional Wave Velocity in Partially Molten Peridotite at High Pressures*. Year Book Carnegie Institute, Washington, DC.
Murase, T., Kushiro, I. and Fujii, T., 1977. Compressional wave velocity in partially molten peridotite. In: *Annual Report of the Director Geophysical Laboratory*. Carnegie Inst., Washington D.C.
Muraveva, N.S. and Senin, V.G., 2009. Carbonate-silicate equilibria in the high-magnesia ultrapotassic volcanics of the Toro-Ankole Province (East African Rift Zone). *Geochem. Int.*, **47**, 882–900.
Nakanishi, I. and Anderson, D.L., 1984. Aspherical heterogeneity of the mantle from phase velocities of mantle waves. *Nature*, **307**, 117–121.
Nataf, H.C., Nakanishi, I. and Anderson, D.L., 1984. Anisotropy and shear-velocity heterogeneities in the upper mantle. *Geophys. Res. Lett.*, **11**, 109–112.
Ni, H., Keppler, H. and Behrens, H., 2011. Electrical conductivity of hydrous basaltic melts: implications for partial melting in the upper mantle. *Contrib. Miner. Petrol.*, **162**, 637–650.
Niu, Y., Collerson, K.D., Batiza, R., Wendt, J.I. and Regelous, M., 1999. Origin of enriched-type mid-ocean ridge basalt at ridges far from mantle plumes: The East Pacific Rise at 11°20′ N. *J. Geophys. Res. B*, **104**, 7067–7087.
Nolet, G., 1985. Nolet, G., Solving or resolving inadequate and noisy tomographic systems. *J. Comput. Phys.*, **61**, 463–482.
Nolet, G., 2008. *A Breviary of Seismic Tomography*. Cambridge University Press, Cambridge.
Obrebski, M., Allen, R.M., Pollitz, F. and Hung, S.H., 2011. Lithosphere-asthenosphere interaction beneath the western United States from the joint inversion of body-wave traveltimes and surface-wave phase velocities. *Geophys. J. Int.*, **185**, 1003–1021.
O'Donnell, J.P., Daly, E., Tiberi, C., Bastow, I.D., O'Reilly, B.M., Readman, P.W. and Hauser, F., 2011. Lithosphere-asthenosphere interaction beneath Ireland from joint inversion of teleseismic P-wave delay times and GRACE gravity. *Geophys. J. Int.*, **184**, 1379–1396.
Oyarzun, R., 1997. Opening of the central Atlantic and asymmetric mantle upwelling phenomena: Implications for long-lived magmatism in western North Africa and Europe. *Geology*, **25**, 727–730.
Paige, C.C. and Saunders, M.A., 1982. LSQR: an algorithm for sparse linear equations and sparse least squares. *Assoc. Comput. Mach. Trans. Math. Software*, **8**, 43–71.
Panning, M.P., Lekic, V. and Romanowicz, B.A., 2010. The importance of crustal corrections in the development of a new global model of radial anisotropy. *J. Geophys. Res.*, **11**, 5.
Panza, G.F., Peccerillo, A., Aoudia, A. and Farina, B., 2007. Geophysical and petrological modelling of the structure and composition of the crust and upper mantle in complex geodynamic settings: the Tyrrhenian Sea and surroundings. *Earth Sci. Rev.*, **80**, 1–46.
Panza, G.F., Doglioni, C. and Levshin, A., 2010. Asymmetric ocean basins. *Geology*, **38**, 59–62.

Paul, A., Hatzfeld, D., Kaviani, A., Tatar, M. and Pequegnat, C., 2010. Seismic imaging of the lithospheric structure of the Zagros mountain belt (Iran). In: *Tectonic and Stratigraphic Evolution of Zagros and Makran during the Mesozoic-Cenozoic* (P. Leturmy and C. Robin, eds). Geological Society, London.

Pik, R., Marty, B. and Hilton, D.R., 2006. How many mantle plumes in Africa? The geochemical point of view *Chem. Geol.*, **226**, 100–114.

Pilidou, S., Priestley, K., Gudmundsson, O. and Debayle, E., 2004. Upper mantle S-wave speed heterogeneity and anisotropy beneath the North Atlantic from regional surface wave tomography: the Iceland and Azores plumes. *Geophys. J. Int.*, **159**, 1057–1076.

Pilidou, S., Priestley, K.F., Debayle, E. and Gudmundsson, O., 2005. Rayleigh wave tomography in the North Atlantic: high resolution images of the Iceland, Azores and Eifel mantle plumes. *Lithos*, **79**, 453–474.

Piromallo, C., Gasperini, D., Macera, P. and Faccenna, C., 2008. A late Cretaceous contamination episode of the European-Mediterranean mantle. *Earth Planet. Sci. Lett.*, **268**, 15–27.

Polet, J. and Anderson, D., 1995. Depth extent of cratons as inferred from tomographic studies. *Geology*, **23**, 205–208.

Poupinet, G., 1979. On the relation between P-wave travel time residuals and the age of the continental plates. *Earth Planet. Sci. Lett.*, **43**, 149–161.

Poupinet, G., Arndt, N. and Vacher, P., 2003. Seismic tomography beneath stable regions and the origin and composition of the continental lithospheric mantle. *Earth Planet. Sci. Lett.*, **212**, 89–101.

Presnall, D. and Gudmundsson, G., 2011. Oceanic volcanism from the low-velocity zone – without mantle plumes. *J. Petrol.*, **52**, 1533–1546.

Priestley, K.F. and Debayle, E., 2003. Seismic evidence for a moderately thick lithosphere beneath the Siberian Platform. *Geophys. Res. Lett.*, **30**, 1118–1122.

Rawlinson, N. and Fishwick, S., 2012. Seismic structure of the southeast Australian lithosphere from surface and body wave tomography. *Tectonophysics*, **572**, 111–122.

Raykova, R.B. and Panza, G.F., 2010. The shear-wave velocity structure of the lithosphere-asthenosphere system in the Iberian area and surroundings. In: *Rend. Fis. Acc. Lincei.*, **21**, 183–231.

Ritsema, J., van Heijst, H.J. and Woodhouse, J.H., 1999. Complex shear wave velocity structure imaged beneath Africa and Iceland. *Science*, **286**, 1925–1928.

Ritsema, J., van Heijst, H.J. and Woodhouse, J.H., 2004. Global transition zone tomography. *J. Geophys. Res.*, **109**, doi:10.1029/2003JB002610.

Ritsema, J., van Heijst, H.J., Deuss, A. and Woodhouse, J.H., 2011. S40RTS: a degree-40 shear velocity model for the mantle from new Rayleigh wave dispersion, teleseismic traveltimes, and normal-mode splitting function measurements. *Geophys. J. Int.*, **184**, 1223–1236.

Ritter, J.R.R., Jordan, M., Christensen, U.R. and Achauer, U., 2001. A mantle plume below the Eifel volcanic fields, Germany. *Earth Planet. Sci. Lett.*, **186**, 7–14.

Ritzwoller, M.H., Shapiro, N.M., Levshin, A.L. and Leahy, G.M., 2001. Crustal and upper mantle structure beneath Antarctica and surrounding oceans. *J. Geophys. Res.*, **106**, 30645–30670.

Ritzwoller, M.H., Shapiro, N.M., Barmin, M.P. and Levshin, A.L., 2002. Global surface wave diffraction tomography. *J. Geophys. Res.*, **107**, 2335.

Rosenthal, A., Foley, S.F., Pearson, D.G., Nowell, G.M. and Tappe, S., 2009. Petrogenesis of strongly alkaline primitive volcanic rocks at the propagating tip of the western branch of the East African Rift. *Earth Planet. Sci. Lett.*, **284**, 236–248.

Sambridge, M.S., 1999a. Geophysical Inversion with a Neighbourhood Algorithm –I. Searching a parameter space. *Geophys. J. Int.*, **138**, 479–494.

Sambridge, M.S., 1999b. Geophysical Inversion with a Neighbourhood Algorithm –II. Appraising the ensemble. *Geophys. J. Int.*, **138**, 727–746.

Scherstén, A., Elliott, T., Hawkesworth, C. and Norman, M., 2004. Tungsten isotope evidence that mantle plumes contain no contribution from the Earth's core. *Nature*, **427**, 234–237.

Schmeling, H., 1985. Numerical model of partial melt on elastic, anelastic and electric properties of rocks, Part I. Elasticity and anelasticity. *Phys. Earth Planet. Inter.*, **41**, 34–57.

Shapiro, N.M. and Ritzwoller, M.H., 2002. Monte-Carlo inversion for a global shear velocity model of the crust and upper mantle. *Geophys. J. Int.*, **151**, 88–105.

Shaw, H.R., 1973. Mantle convection and volcanic periodicity in the Pacific; evidence from Hawaii. *Geol. Soc. Am. Bull.*, **84**, 1505–1526.

Silveira, G. and Stutzmann, E., 2002. Anisotropic tomography of the Atlantic ocean. *Phys. Earth Planet. Inter.*, **132**, 237–248.

Simons, F.J., Zielhuis, A. and van der Hilst, R.D., 1999. The deep structure of the Australian continent from surface wave tomography. *Lithos*, **48**, 17–43.

Song, T.R.A. and Helmberger, D.V., 2007. Validating tomographic models with broad-band waveform modelling: an example from the LA RISTRA transect in the southwestern United States. *Geophys. J. Int.*, **171**, 244–258.

Spencer, C. and Gubbins, D., 1980. Travel-time inversion for simultaneous earthquake location and velocity structure determination in laterally varying media. *Geophys. J. Roy. Astron. Soc.*, **63**, 95–116.

Stracke, A., 2012. Earth's heterogeneous mantle: A product of convection-driven interaction between crust and mantle. *Chem. Geol.*, **330-331**, 274–299.

Stracke, A., Hofmann, A.W. and Hart, S.R., 2005. FOZO, HIMU, and the rest of the mantle zoo. *Geochem. Geophys. Geosyst.*, **6**, doi:10.1029/2004GC000824.

Stuart, F.M., Lass-Evans, S., Fitton, J.G. and Ellam, R.M., 2003. High $^3He/^4He$ ratios in picritic basalts from Baffin Island and the role of a mixed reservoir in mantle plumes. *Nature*, **424**, 57–59.

Sumino, Y. and Anderson, O.L., 1982. Elastic constants in minerals. In: *CRC Handbook of Physical Properties of Rocks* (R.S. Carmichel, ed.). CRC Press, Boca Raton, Fla.

Sun, D. and Helmberger, D., 2011. Upper-mantle structures beneath USArray derived from waveform complexity. *Geophys. J. Int.*, **184**, 416–438.

Tanimoto, T. and Anderson, D.L., 1984. Mapping convection in the mantle. *Geophys. Res. Lett.*, **11**, 287–290.

Tappe, S., Foley, S.F. and Pearson, D.G., 2003. The kamafugites of Uganda: a mineralogical and geochemical comparison with their Italian and Brazilian analogues. *Periodico di Mineralogia*, **72**, 51–77.

Tarantola, A., 1987. *Inverse Problem Theory*. Elsevier Science Ltd, Amsterdam.

Thurber, C.H., 1993. Local earthquake tomography: velocities and Vp/Vs – theory. In: *Seismic Tomography: Theory and Applications* (H.M. Iyer and K. Hirahara, eds). Chapman and Hall, London.

Thybo, H., 2006. The heterogeneous upper mantle low velocity zone. *Tectonophysics*, **416**, 53–79.

Thybo, H. and Perchuc, E., 1997. The seismic 8° discontinuity and partial melting in continental mantle. *Science*, **275**, 1626–1629.

Trampert, J. and Spetzler, J., 2006. Surface wave tomography: finite frequency effects lost in the null space. *Geophys. J. Int.*, **164**, 394–400.

Trampert, J. and van der Hilst, R.D., 2005. Towards a quantitative interpretation of global seismic tomography. *Geophys. Monogr.*, **160**, 47–62.

Trampert, J. and Woodhouse, J.H., 1995. Global phase velocity maps of Love and Rayleigh waves between 40 and 150 s. *Geophys. J. Int.*, **122**, 675–690.

Trampert, J., Deschamps, F., Resovsky, J. and Yuen, D., 2004. Probabilistic tomography maps chemical heterogeneities throughout the lower mantle. *Science*, **306**, 853–856.

Tumanian, M., Frezzotti, M.L., Peccerillo, A., Brandmayr, E. and Panza, G.F., 2012. Thermal structure of the shallow upper mantle beneath Italy and neighbouring areas: Correlation with magmatic activity and geodynamic significance. *Earth Sci. Rev.*, **114**, 369–385.

Van Der Lee, S. and Nolet, G., 1997. Seismic image of the subducted trailing fragments of the Farallon plate. *Nature*, **386**, 266–269.

VanDecar, J.C. and Crosson, R.S., 1990. Determination of teleseismic relative phase arrival times using multi-channel cross-correlation and least squares. *Bull. Seismol. Soc. Am.*, **80**, 150–169.

VanDecar, J.C., James, D.E. and Assumpcao, M., 1995. Seismic evidence for a fossil mantle plume beneath south America and implications for plate driving forces. *Nature*, **378**, 25–31.

Wawerzinek, B., Ritter, J.R.R., Jordan, M. and Landes, M., 2008. An upper-mantle upwelling underneath Ireland revealed from non-linear tomography. *Geophys. J. Int.*, **175**, 253–268.

Webber, A.P., Roberts, S., Taylor, R.N. and Pitcairn, I.K., 2013. Golden plumes: substantial gold enrichment of oceanic crust during ridge-plume interaction. *Geology*, **418**, 7–90.

White, W.M., 2010. Oceanic Island Basalts and mantle plumes: the geochemical perspective. *Annu. Rev. Earth Planet. Sci.*, **38**, 133–160.

Wolfe, C.J., Solomon, S.C., Laske, G., Collins, J.A., Detrick, R.S., Orcutt, J.A., Bercovici, D. and Hauri, E.H., 2009. Mantle shear-wave velocity structure beneath the Hawaiian hot spot. *Science*, **326**, 1388–1390.

Wolfe, C.J., Solomon, S.C., Laske, G., Collins, J.A., Detrick, R.S., Orcutt, J.A., Bercovici, D. and Hauri, E.H., 2011. Mantle P-wave velocity structure beneath the Hawaiian hotspot. *Earth Planet. Sci. Lett.*, **303**, 267–280.

Woodhouse, J.H. and Dziewonski, A.M., 1984. Mapping the upper mantle: Three-dimensional modeling of Earth structure by inversion of seismic waveforms. *J. Geophys. Res.*, **89**, 5953–5986.

Wyllie, P.J., 1988. Magma genesis, plate tectonics and chemical differentiation of the Earth. *Rev. Geophys.*, **26**, 370–404.

Yang, Y., Ritzwoller, M.H., Levshin, A.L. and Shapiro, N.M., 2007. Ambient noise Rayleigh wave tomography across Europe. *Geophys. J. Int.*, **168**, 259–274.

Yanovskaya, T.B., 1997. Resolution estimation in the problems of seismic ray tomography, Izvestiya. *Phys. Solid Earth*, **33**, 762–765.

Yanovskaya, T.B., 2009. Surface wave tomography method based on data from distant earthquakes, Izvestiya. *Phys. Solid Earth*, **45**, 225–230.

Yanovskaya, T.B. and Kozhevnikov, V.M., 2003. 3D S-wave velocity pattern in the upper mantle beneath the continent of Asia from Rayleigh wave data. *Phys. Earth Planet. Inter.*, **138**, 263–278.

Yuan, H. and Dueker, K.G., 2005. Teleseismic P-wave tomogram of the Yellowstone plume. *Geophys. Res. Lett.*, **32**, doi:10.1029/2004GL022056.

Zhou, H. and Dick, H.J.B., 2013. Thin crust as evidence for depleted mantle supporting the Marion Rise. *Nature*, **494**, 195–200.

Zindler, A. and Hart, S.R., 1986. Chemical Geodynamics. *Annu. Rev. Earth Planet. Sci.*, **14**, 493–571.

Received 15 February 2013; revised version accepted 2 March 2013

Supporting Information

Additional Supporting Information may be found in the online version of this article:

Figure S1: Schematic of a portion of one typical kernel (column) of **R** for a block or node at the centre of layer *n* for a typical teleseismic tomography study (grey lines and dots) showing the relative magnitudes of diagonal (black dot) and off-diagonal (grey dots) elements of **R**. These dots are (horizontally) at block centres and vertically proportional to the amplitude of **R** in that element (relative scale at left). Such representations can be thought of as the "impulse response" to the presence of a single-block anomaly at the centre of layer *n*, for the filter comprising a particular dataset and (to a lesser degree) the particular inversion method used.

Figure S2: Typical but idealized two-dimensional ray set for teleseismic tomography. Arbitrary scaling; no vertical exaggeration (after Evans and Achauer, 1993).

Figure S3: Two-dimensional synthetic-data tests of resolution for (*a*) a best-case and (*b*) more typical ray sets, with similar numbers of rays in each. The models used to create synthetic travel times are in (*c*), (*f*), (*i*), and (*l*). Inversion results using the best-case ray set are in (*d*), (*g*), (*j*), and (*m*) and those for the more typical ray set are in (*e*), (*h*), (*k*), and (*n*). Green ovals in (*a*) and (*b*) are estimated minimum-resolvable objects in various locations (from Yanovskaya, 1997).

Figure S4: Synthetic wave-speed model for the Ethiopian rift (left) consisting of high wave speed ($\Delta vP = 5\%$) rift flanks. A relative arrival-time dataset is computed for the same station-earthquake pairs used in the study of Bastow *et al.* (2008). The resulting tomographic model is characterized not only by high-wave-speed flanks but also by a low-wave-speed zone beneath the rift valley. In reality, in Ethiopia, *P*- and *S*-wave arrival times are ubiquitously late compared with the global mean, with the implication that the "high" wave-speed (blue) regions are low wave-speed compared with the global mean (Bastow *et al.*, 2008; Bastow, 2012). A model result with high and low wave-speed structure is the inevitable consequence of relative arrival-time inversions.

